© 2022. Published by The Company of Biologists Ltd | Development (2022) 149, dev200717. doi:10.1242/dev.200717

HUMAN DEVELOPMENT

RESEARCH ARTICLE

Dysregulation of integrin αvβ3 and α5β1 impedes migration of placental endothelial cells in fetal growth restriction

Diane L. Gumina[1], Shuhan Ji[1], Amanda Flockton[1], Kathryn McPeak[1], Dominik Stich[2], Radu Moldovan[2] and Emily J. Su[1,3,*]

ABSTRACT

Placentas from pregnancies complicated by severe early-onset fetal growth restriction (FGR) exhibit diminished vascular development mediated by impaired angiogenesis, but underlying mechanisms remain unknown. In this study, we show that FGR endothelial cells demonstrate inherently reduced migratory capacity despite the presence of fibronectin, a matrix protein abundant in placental stroma that displays abnormal organization in FGR placentas. Thus, we hypothesized that aberrant endothelial-fibronectin interactions in FGR are a key mechanism underlying impaired FGR endothelial migration. Using human fetoplacental endothelial cells isolated from uncomplicated term control and FGR pregnancies, we assessed integrin α5β1 and αvβ3 regulation during cell migration. We show that endothelial integrin α5β1 and αvβ3 interactions with fibronectin are required for migration and that FGR endothelial cells responded differentially to integrin inhibition, indicating integrin dysregulation in FGR. Whole-cell expression was not different between groups. However, there were significantly more integrins in focal adhesions and reduced intracellular trafficking in FGR. These newly identified changes in FGR endothelial cellular processes represent previously unidentified mechanisms contributing to persistent angiogenic deficiencies in FGR.

KEY WORDS: Placental dysfunction, Endothelial cells, Integrins, Fetal growth restriction, Angiogenesis, Human

INTRODUCTION

Fetal growth restriction (FGR) is diagnosed via ultrasound when an estimated fetal weight is less than the 10th percentile for gestational age. In general, FGR increases the risk for short- and long-term complications. These risks, including stillbirth, neonatal demise, prematurity and other long-term health consequences such as cardiometabolic diseases, are further increased in the setting of severe early-onset FGR (Baschat et al., 2000; Crimmins et al., 2014; Pisaneschi et al., 2013; Thornton et al., 2004). Severe FGR is associated with substantial placental dysfunction, and pregnancies meet criteria for this diagnosis when the estimated fetal weight or abdominal circumference is less than the 3rd percentile for gestational age and/or if umbilical artery Doppler velocimetry, which represents placental vascular resistance, is elevated (Gordijn et al., 2016; Martins et al., 2020). However, it is the presence of extremely high placental vascular resistance, clinically evident by absent or reversed umbilical artery Dopplers, that truly increases risk for adverse perinatal and long-term outcomes (Alfirevic et al., 2017; Nicolaides et al., 1988; Pardi et al., 2010).

Normally, because the placenta is an organ with low vascular resistance, the umbilical arteries exhibit forward flow at all points of the fetal cardiac cycle. This unimpeded umbilical blood flow is the result of ongoing angiogenesis throughout the latter half of pregnancy, which generates a lushly branched vascular tree allowing for a normal and progressive decrease in fetoplacental vascular resistance across gestation. However, abnormally increased fetoplacental vascular resistance, a key manifestation of placental dysfunction in cases of severe FGR, is a consequence of inadequate angiogenesis, where terminal villous vessels display a lack of branching and are abnormally thin and elongated. This morphology results in diminished forward velocity during fetal cardiac diastole, potentially progressing to absent or even reversed end-diastolic velocities (Baschat et al., 2001). These placental alterations associated with FGR ultimately lead to decreased vessel surface area, resulting in impaired nutrient and gas exchange between the fetal and maternal circulations, while also adding substantial strain to the fetal heart (Jackson et al., 1995; Krebs et al., 1996; Salafia et al., 1997; Todros et al., 2011). Together, these pathophysiologic consequences contribute to substantially increased risk for adverse perinatal and long-term outcomes. However, the cellular and molecular mechanisms underlying impaired placental angiogenesis remain unknown.

We have previously published research showing that endothelial cells isolated from severe FGR placentas exhibit reduced angiogenic function *in vitro*, with diminished migratory capacity and reduced ability to form capillary-like structures (Ji et al., 2019; Su et al., 2015). These findings underscore that placental endothelial cells isolated from FGR placentas maintain inherent impairments even when removed from the *in utero* environment. However, angiogenesis is not driven by endothelial cells alone, and understanding how interactions with the placental microenvironment influence angiogenic capacity is key to identifying mechanisms responsible for diminished vascular development associated with FGR.

Placental villous stroma is a fundamental yet significantly understudied component of the placental microenvironment. The hypothesis that placental villous stromal extracellular matrix (ECM) regulates fetoplacental vascular development is supported by the following four points. First, endothelial cell-ECM interactions are crucial in regulating tumor angiogenesis (Balcioglu et al., 2016; De Palma et al., 2017). Second, placental endothelial cells directly interact with villous stromal matrix (Sankaran, 2012). Third, FGR

[1]Division of Reproductive Sciences, Department of Obstetrics and Gynecology, University of Colorado School of Medicine, Aurora, CO 80045, USA. [2]Department of Pharmacology, University of Colorado School of Medicine, Aurora, CO 80045, USA. [3]Division of Maternal-Fetal Medicine, Department of Obstetrics and Gynecology, University of Colorado School of Medicine, Aurora, CO 80045, USA.

*Author for correspondence (emily.su@cuanschutz.edu)

D.L.G., 0000-0001-9408-9701; S.J., 0000-0002-3992-656X; K.M., 0000-0003-2942-0423; D.S., 0000-0002-7166-8759; E.J.S., 0000-0003-3739-9396

Handling Editor: Liz Robertson
Received 3 March 2022; Accepted 23 August 2022

Development (2022) 149, dev200717. doi:10.1242/dev.200717

placentas have significantly less stromal volume when compared with healthy controls (Chen and Aplin, 2003; Sağol et al., 2002). Fourth, our lab has previously demonstrated that ECM derived from FGR placental fibroblasts inhibits control endothelial cell proliferation and migration, whereas ECM generated from control placental fibroblasts partially rescues FGR endothelial cell angiogenic properties (Ji et al., 2021). Together, these data suggest that stromal ECM deficiencies, through endothelial cell-matrix interactions, contribute specifically to FGR pathophysiology.

Fibronectin is crucial for vessel remodeling in various vascular models and, within the placental villous stroma, it is one of the most abundant ECM components (Chen and Aplin, 2003; Zhou et al., 2008). Furthermore, fibronectin organization is abnormal in ECM generated from FGR placental fibroblasts (Ji et al., 2021). The two main fibronectin-binding integrins expressed by endothelial cells are αvβ3 and α5β1. These integrins are implicated in regulating angiogenesis but have not yet been investigated in fetoplacental endothelial function. Integrins αvβ3 and α5β1 initiate wide-ranging signaling cascades that regulate survival and actin cytoskeleton dynamics, both of which are key aspects of cellular migration (Byzova et al., 1998; Clark et al., 1996; Rüegg and Mariotti, 2003). Moreover, coordination between integrin αvβ3 and α5β1 signaling is necessary for regulating angiogenic processes (Diaz et al., 2020). These data suggest that, in the placenta, endothelial integrin αvβ3 and α5β1 interaction with villous stromal fibronectin may be an important contributing factor to placental angiogenesis. Thus, our objective was to delineate the role of fetoplacental endothelial cell fibronectin-binding integrins in placental angiogenesis, and we hypothesized that impaired migration in FGR placental endothelial cells is mediated by aberrant integrin αvβ3 and α5β1 interaction with fibronectin.

RESULTS

Subject characteristics

All FGR subjects exhibited either absent or reversed end-diastolic umbilical artery Doppler velocimetry. The comparison of subject characteristics (Table 1) demonstrates that there were no significant differences between groups except for gestational age at time of delivery and birthweight percentile. Both results were expected as standard of care is to deliver all cases of severe FGR with absent or reversed umbilical artery Dopplers no later than 34 weeks gestation. All pregnancies were spontaneously conceived and not the result of *in vitro* fertilization. Furthermore, all individuals who had a history of tobacco, alcohol, cannabis or illicit drug use during pregnancy were ineligible for recruitment.

Table 1. Subject demographics

	Controls (*n*=6)	FGR (*n*=6)	*P*-value
Maternal age	33.2±1.8	30.5±1.8	0.3146
Nulliparity	1	3	0.5455*
Maternal BMI	26.2±1.7	30.1±4.0	0.3883
Maternal race			0.2998*
Asian	0	1	
Hispanic/Latina	1	0	
White	4	2	
Unknown	1	3	
Gestational age at delivery	39.1±0.1	29.1±1.5	**0.0022**‡
Fetal sex			
Female	3 (50%)	3 (50%)	>0.9999
Male	3 (50%)	3 (50%)	>0.9999
Birthweight percentile	59.8±7.8	4.6±2.1	**<0.0001**
Cesarean section	100% (6)	100% (6)	>0.9999
Absent umbilical artery end-diastolic velocities	n/a	66% (4)	
Reversed umbilical artery end-diastolic velocities	n/a	33% (2)	

*Fisher's exact test was used for categorical data. ‡Mann–Whitney *U*-test was performed for non-normally distributed data. Unpaired *t*-tests were used for all other comparisons.
Significant values are represented with bold font.

Integrin α5β1 and αvβ3 interactions with fibronectin are required for placental endothelial cell migration

We had previously shown that FGR endothelial cells exhibit reduced migratory capacity in the absence of any exogenous substrate (Ji et al., 2021). However, whether this phenotype would persist when cells were exposed to exogenous fibronectin or if fibronectin could improve FGR migration was unknown. After plating cells on equal amounts of fibronectin, we found that FGR endothelial cell migration remained impaired, demonstrating that this substrate alone was inadequate to rescue FGR angiogenesis (Fig. 1).

Thus, to determine whether FGR migratory defects were regulated by endothelial cell interactions with fibronectin, FGR and control cells plated on fibronectin were treated with one of three blocking antibodies that inhibit the active forms of fibronectin-binding integrins α5, β1 or αvβ3, or they were subjected to isotype controls. There were no significant differences in migration between untreated and IgG-treated cells (Fig. S1). Both control and FGR endothelial cells treated with either AIIB2 (integrin β1 blocking antibody) or JBS5 (integrin α5 blocking antibody) showed significant impairment in migration when compared with their respective isotype controls. When directly comparing treated FGR and treated control, there was a significant migratory impairment in FGR endothelial cells subjected to integrin α5 or β1 inhibition (Fig. 2A,B), suggesting either increased FGR sensitivity to α5β1 inhibition or alternatively, baseline reduction of FGR migratory capacity. However, integrin αvβ3 inhibition with LM609 treatment resulted in differential effects on control and FGR cells. As anticipated, when compared with IgG-treated cells, control cells exposed to LM609 exhibited significantly impaired migration to a degree similar to FGR cells at baseline. Most notably, however, αvβ3 inhibition of FGR endothelial cells did not significantly affect migration as compared with isotype-control treated FGR cells, suggesting that FGR endothelial cells are not able to effectively use αvβ3 (Fig. 2C). Representative images of percent relative wound density (%RWD) over time for all FGR and control subject conditions are provided in Fig. S2.

FGR migratory impairment is not caused by reduced expression of integrins αvβ3 and α5β1

Inhibiting integrins α5, β1 and αvβ3 activation in a scratch wound assay confirmed that these main fibronectin-binding integrins were required for placental endothelial cell migration. To understand if the migratory defect associated with FGR was caused by differences in integrin α5β1 and αvβ3 expression, qPCR was used to investigate differences in gene expression, and capillary immunoblot was used to quantify protein expression. Both experiments showed no significant differences in gene or protein expression when control and FGR endothelial cells were plated on fibronectin (Fig. 3). Fig. S3 shows the entire immunoblot and the statistical comparisons demonstrating no significant differences in the protein loading control.

Development (2022) 149, dev200717. doi:10.1242/dev.200717

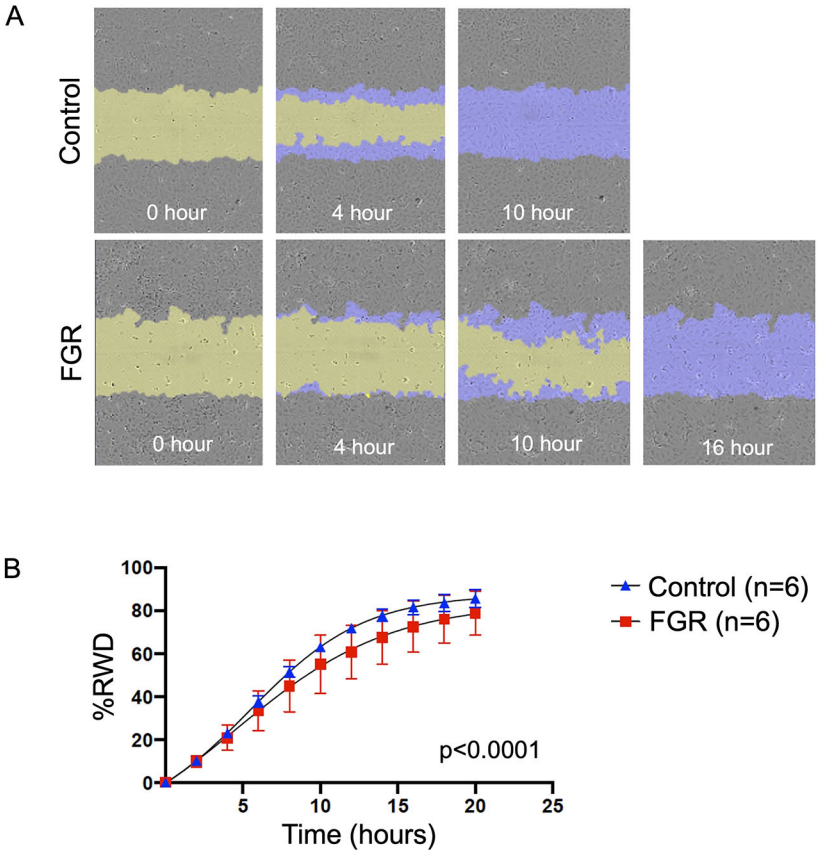

Fig. 1. FGR endothelial cell migratory impairment persists in the setting of exogenous fibronectin substrate. (A) Representative images of percent relative wound density (%RWD) with automated image analyses over 24 h for control and FGR endothelial cells plated on fibronectin. (B) Comparison of migratory capacity of control and FGR subjects plated on fibronectin showed a significant reduction in FGR endothelial cell migration compared with control cells (P<0.0001; non-linear regression). Subject number of n=6 per group. Data are mean±s.e.m. Experiments were repeated in triplicate, with at least four technical replicates per subject per condition.

Post-translational regulation of integrins

Migratory impairments in response to inhibition of integrins αvβ3 and α5β1 observed in Fig. 2 demonstrate that control placental endothelial cells require both integrin heterodimers for migration. Although the impaired migratory response seen in FGR endothelial cells was not explained by differences in total endothelial cell αvβ3 or α5β1 gene or protein expression, other modes of integrin regulation may be implicated. Integrin signaling is highly dynamic and tightly regulated by additional mechanisms such as heterodimer activation, focal adhesion complex formation and intracellular trafficking dynamics. The experiments presented in Figs 4, 5 and 6 explore potential differences between control and FGR post-translational regulation of integrin αvβ3 and α5β1.

FGR and control endothelial cells display similar amounts of active integrin αvβ3 and α5β1

Integrin activation is one mechanism by which cells regulate integrin function through their affinity for ligands such as fibronectin. Activation results in signaling that further regulates various cellular events, including adhesion, polarity and migration. Integrin heterodimers exist in either the active or inactive conformation at the cell surface. As one example, intracellular signals can maintain the heterodimer in its bent, closed, inactive conformation, whereas inhibition of these inactivators pushes the integrin heterodimer to assume an extended conformation, allowing it to bind to specific ECM proteins.

To determine whether αvβ3 or α5β1 activation was affected in FGR endothelial cells, integrin-based adhesions and complexes containing active integrins bound to substrate were isolated and assayed via immunoblot as described previously (Jones et al., 2015) (Fig. S4). As demonstrated in Fig. S5, we were able to successfully isolate active integrins from placental endothelial cells. Proof-of-concept experiments demonstrated that isolated proteins were substrate-specific and free of unintended cellular components, indicating that these protocol adaptations were successful in placental endothelial cells. Specifically, when endothelial cells were plated on fibronectin, integrin αv and β3 subunits were both enriched, compared with cells plated on the negative control substrate apotransferrin. There was also further enrichment when endothelial cells were subjected to both fibronectin and 1 mM manganese chloride ($MnCl_2$), a divalent cation that promotes high integrin affinity. Likewise, transferrin receptor was enriched only in apotransferrin-coated conditions whereas integrin α2, a collagen-specific integrin, was enriched only when cells were plated on collagen. Probing for PCNA, a nuclear protein, demonstrated that isolates were free from cellular contamination. In contrast, vinculin, an intracellular protein recruited by active integrins, was present only in the setting of fibronectin and not with apotransferrin, as was the transmembrane protein vascular endothelial growth factor receptor 2 (VEGFR2; also known as KDR). Together, the presence of both vinculin and VEGFR2 was further confirmation that integrin signaling hubs remained fully intact. Using this technique, there were no significant differences in integrin αv, α5, β1 and β3 subunits when comparing isolates from FGR and controls at 2.5 h after cell plating (Fig. 4). This demonstrates that, at this single time point, differential activation of αvβ3 or α5β1 at the membrane does not explain the migratory defects in FGR endothelial cells.

Integrin α5β1 and αvβ3 focal adhesion complexes are altered in FGR endothelial cells

Another important mode of integrin regulation is the formation of focal adhesion complexes. Focal adhesion formation includes integrin heterodimers that have bound to the appropriate ECM protein and have recruited intracellular proteins, other integrin

Development (2022) 149, dev200717. doi:10.1242/dev.200717

A

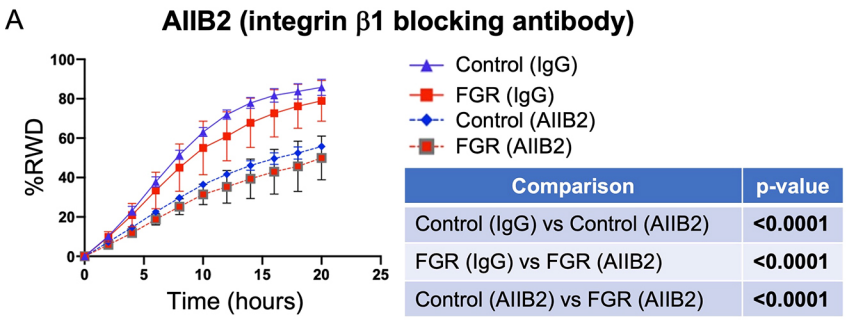

Comparison	p-value
Control (IgG) vs Control (AIIB2)	**<0.0001**
FGR (IgG) vs FGR (AIIB2)	**<0.0001**
Control (AIIB2) vs FGR (AIIB2)	**<0.0001**

B

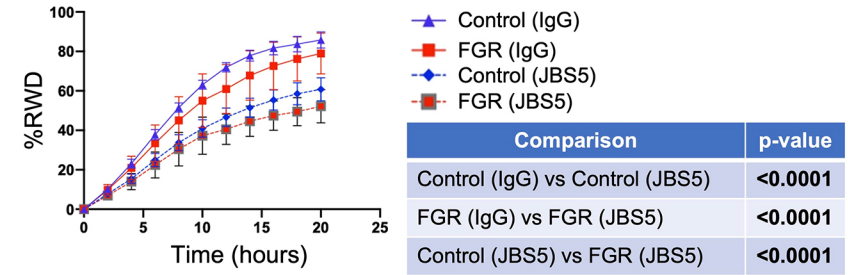

Comparison	p-value
Control (IgG) vs Control (JBS5)	**<0.0001**
FGR (IgG) vs FGR (JBS5)	**<0.0001**
Control (JBS5) vs FGR (JBS5)	**<0.0001**

C

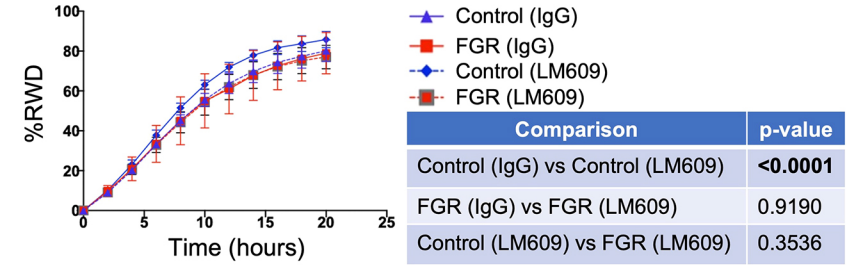

Comparison	p-value
Control (IgG) vs Control (LM609)	**<0.0001**
FGR (IgG) vs FGR (LM609)	0.9190
Control (LM609) vs FGR (LM609)	0.3536
FGR (IgG) vs Control (LM609)	0.9073

Fig. 2. Integrin αvβ3 is ineffectively used by FGR endothelial cells. (A,B) Endothelial cell surface inhibition of either active integrin α5 (JBS5; B) or active integrin β1 (AIIB2; A) resulted in significantly reduced migration in a scratch wound assay for both control and FGR subjects. (C) Although inhibition of integrin αvβ3 (LM609) significantly reduced control endothelial cell migration to the degree of basal impairment seen in FGR cells, there was no additional effect of αvβ3 blockade on FGR cell migration. All *P*-values are listed in the corresponding tables. Subject number of *n*=6 per group per treatment condition. Data are mean±s.e.m. Non-linear regression was used for statistical comparisons. Experiments were repeated in triplicate, with at least four technical replicates per subject per condition.

heterodimers and other transmembrane proteins, all of which coordinate the amplification of localized signaling. To determine whether aberrant focal adhesion formation was implicated in impaired FGR endothelial migration, we performed a scratch wound assay and assessed cells 3 h after creation of the wound. This experimental design was chosen to capture endothelial cells during active migration.

Focal adhesions have a life cycle, and to identify any differences in integrin-containing immature and mature focal adhesions, paxillin was used as a marker of immature adhesions and zyxin identified those that were mature. Vinculin was considered a surrogate for total focal adhesions. To identify focal adhesions containing active integrins of interest, cells were additionally stained with either JBS5 (active integrin α5 antibody), AIIB2 (active integrin β1 antibody) or LM609 (active integrin αvβ3 antibody). The experimental design, including a list of co-staining conditions, is provided in Fig. 5A. TIRF microscopy images were either separated into single channel grayscale images or processed into binary colocalization images followed by automated analysis of the number of adhesions per image. Between 1200 and 1600 focal adhesions within 8-32 regions of interest (ROI), depending on the antibody stain, were analyzed per subject. We then performed comparisons on the number of focal adhesions for each staining condition between control and FGR endothelial cells.

Similar to the findings presented in Fig. 4, there were no significant differences in the total number of αvβ3-positive focal adhesions. However, there was a significant increase in focal adhesions co-stained with αvβ3-paxillin and αvβ3-vinculin, demonstrating an imbalance in the amount of immature focal adhesions in FGR endothelial cells (Fig. 5B,C). In addition, despite no difference in α5β1 activation in FGR ECs, there was a significant increase in the number of active integrin α5-positive focal adhesions in FGR, which appeared to be mediated at least in part by a significant increase in the amount of α5-zyxin co-stained focal adhesions (Fig. 5D,E). Similarly, there was no difference in the number of active integrin β1-positive focal adhesions in FGR, but there was a significant increase in the number of integrin β1-vinculin co-stained adhesions (Fig. 5F). Together, these data suggest that there is an alteration of focal adhesion maturation that is integrin-specific in FGR endothelial cells. Changes in focal adhesions membrane-level dynamics could potentially drive aberrant signaling of anchorage-dependent events and impair proper establishment of cell polarity, thus contributing to the migratory impairment associated with FGR.

Intracellular endosomal vesicles are reduced in FGR endothelial cells

As our data suggested altered focal adhesion complex maturation for both α5β1 and αvβ3 adhesions in FGR endothelial cells, we sought

Development (2022) 149, dev200717. doi:10.1242/dev.200717

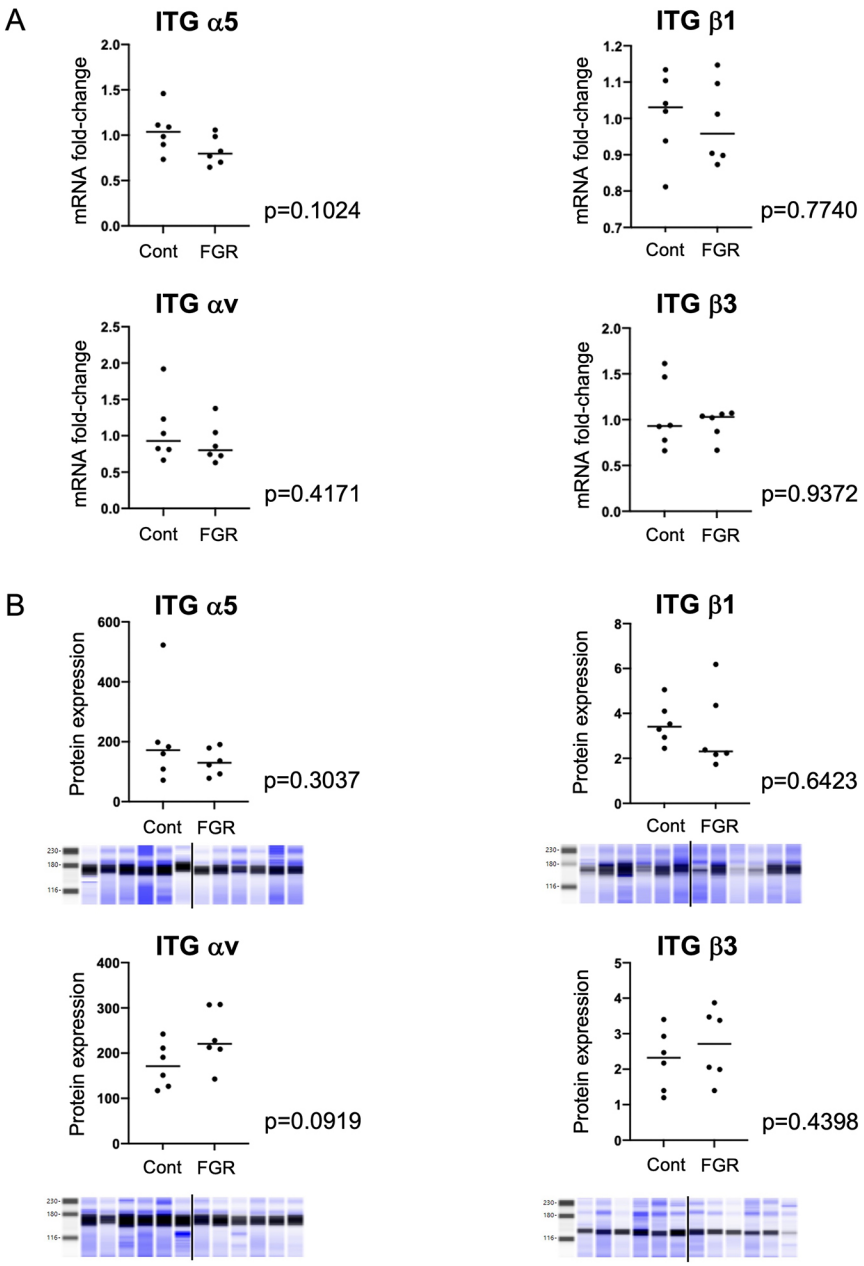

Fig. 3. FGR migratory impairment on fibronectin is not caused by reduced expression of integrins αvβ3 and α5β1. (A) There was no significant difference in mRNA expression of integrins α5, β1, αv and β3 between control and FGR endothelial cells. (B) Via capillary immunoblotting, protein expression of these integrin subunits also did not significantly differ between control and FGR endothelial cells after normalization to total protein stain (shown in blue). Subject number of *n*=6 per group. Unpaired two-tailed Student's *t*-tests were used for statistical comparisons. Horizontal line shows mean. Experiments were repeated in triplicate.

to determine whether these findings extended to inappropriate intracellular trafficking. For cells in locomotion to move forward, new focal adhesions must be established at the leading edge of the cell, while the focal adhesion at the lagging edge must be released and internalized. Once internalized, active integrins are either targeted for lysosomal degradation or recycled back to a new location on the cell membrane (Fig. 6A). Using the same scratch wound experimental design detailed in Fig. 5, confocal microscope images of vesicles stained with the early endosomal marker EEA1 or the late endosomal marker RAB7A were used to determine the number of vesicles per cell. For these analyses, 72 ROI per subject per antibody stain were assessed. These analyses show that there were reduced vesicles per cell for both early and late endosomes (Fig. 6B,C) in FGR, suggesting that altered intracellular trafficking dynamics are present in FGR. There were no differences in the number of internalized vesicles stained with the active integrin markers for αvβ3 (LM609), active integrin α5 (JBS5) or active integrin β1 (AIIB2) (Fig. 6D-F). However, this data is consistent with our findings in Fig. 3, which demonstrated no differences in integrin expression between cohorts. Further future experiments are needed to determine whether reduced endosomal trafficking impairs integrin trafficking.

DISCUSSION

Angiogenic and vasculogenic processes are vital for the development of the placental vasculature. As shown here, FGR endothelial cells display reduced motility, an important cellular process required for successful angiogenesis and vasculogenesis. When considering the morphological findings of reduced placental vasculature associated with FGR, it is possible that this dysfunctional cellular mechanism is a contributing factor.

Our data reveal that, although fibronectin is abundantly expressed in the placental stroma, exogenous fibronectin is not sufficient to rescue FGR placental endothelial cell migratory function, confirming that inherent endothelial cell defects exist in FGR regardless of substrate. Data presented here also show that integrins

Development (2022) 149, dev200717. doi:10.1242/dev.200717

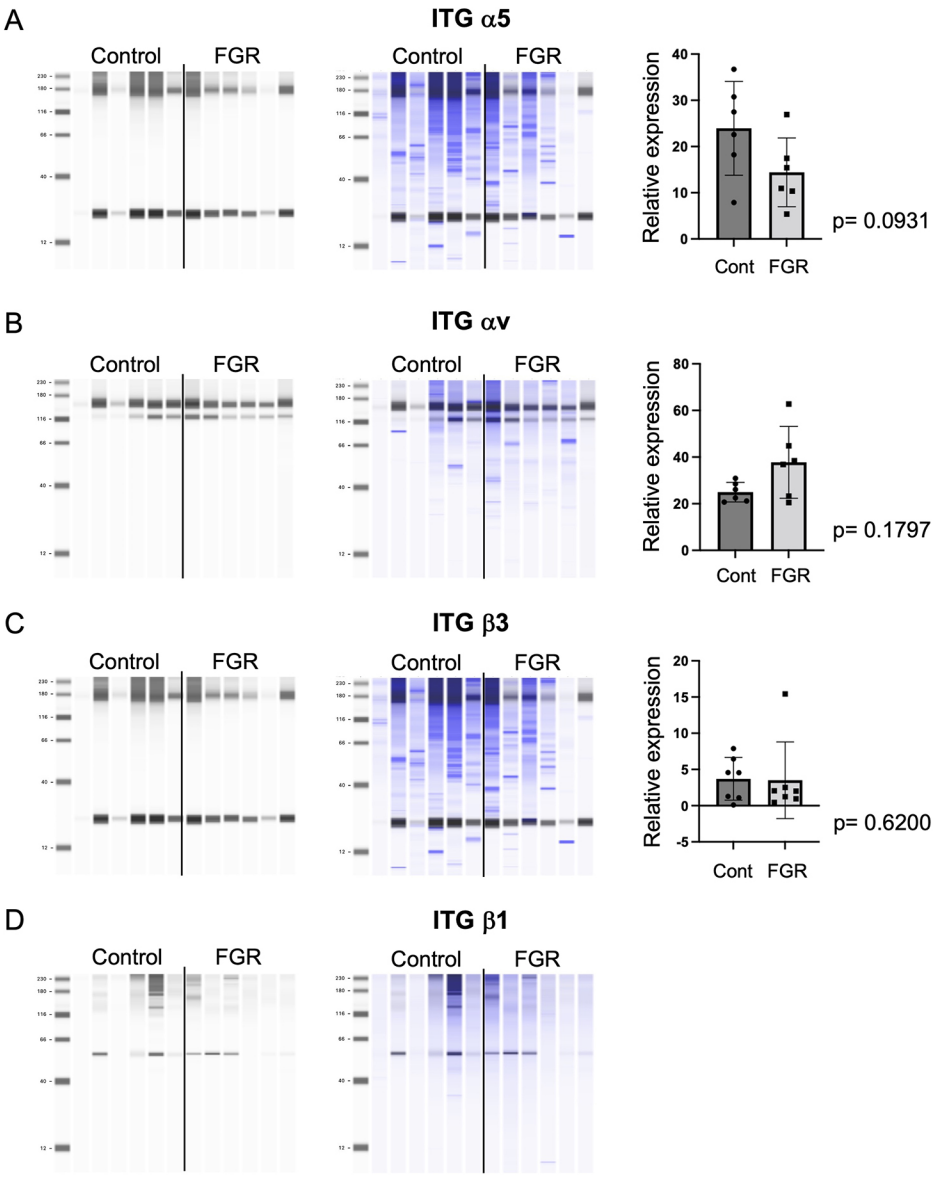

Fig. 4. FGR and control endothelial cells display similar amounts of active integrin α5β1 and αvβ3 at the cell membrane. (A-D) After isolation of integrin-based adhesions and complexes at the cell membrane, samples were probed for integrin α5 (A), integrin αv (B), integrin β3 (C) and integrin β1 (D). Relative expression was quantified after normalization to total protein (shown in blue). Subject number of *n*=6 per group with six plates pooled per subject. Mann–Whitney *U*-tests were used for statistical analysis. Data are mean±s.e.m. Integrin β1 was not analyzed statistically as there was no signal present at the expected molecular weight.

α5β1 and αvβ3 are required for normal placental endothelial cell migration and that dysfunction of these integrins in FGR is not related to reduced gene or protein expression. Rather, other modes of integrin regulation are implicated. Specifically, there are increased active αvβ3 heterodimers in focal adhesions that display significantly more co-staining with immature focal adhesion markers in FGR. In addition, we show that there are increased focal adhesions containing active α5 and β1, with more active α5 co-staining with a mature focal adhesion marker in FGR. Lastly, there appears to be global changes in intracellular trafficking with reduced early and late endosomal vesicles in FGR.

One potential explanation for increased active αvβ3 heterodimers in immature focal adhesions is that the active αvβ3 heterodimer does not recruit the appropriate proteins required to form a mature focal adhesion. Conversely, we found that integrin α5β1 in FGR exhibits increased numbers of α5, α5-zyxin and β1-vinculin positive focal adhesions. This suggests a disruption in two different processes regulating integrin function. One possibility is that these findings are a result of improper outside-in integrin signaling, which is initiated by integrin binding to an ECM ligand, resulting in downstream signaling and focal adhesion complex formation and maturation. Altered outside-in signaling could be responsible for the increased amounts of integrin αvβ3 and α5β1 in focal adhesions and imbalanced focal adhesion maturation seen in FGR. The other possibility is that inside-in signaling, which refers to intracellular trafficking of integrins, is impaired. When considering the findings of reduced early and late endosomes in FGR, it is possible that global impairment of intracellular trafficking in FGR extends to intracellular trafficking of integrin heterodimers and subunits, thereby causing dysfunctional integrin signaling.

These findings support a hypothesis in which integrins α5β1 and αvβ3 are differentially dysregulated in FGR endothelial cells, both of which contribute to the impaired migratory phenotype. However, we acknowledge the potential for even more complex integrin regulation in placental angiogenesis. First, it is important to acknowledge that our experiments only represent a snapshot at a single time point. Yet, the fact that there are clear differences at one time point in a highly dynamic process suggests that these two integrins are indeed dysregulated in FGR. Incorporation of live-cell imaging tools that allow for mapping trajectories of individual focal adhesions will provide a more comprehensive understanding of the specific mechanisms contributing to integrin dysregulation.

Development (2022) 149, dev200717. doi:10.1242/dev.200717

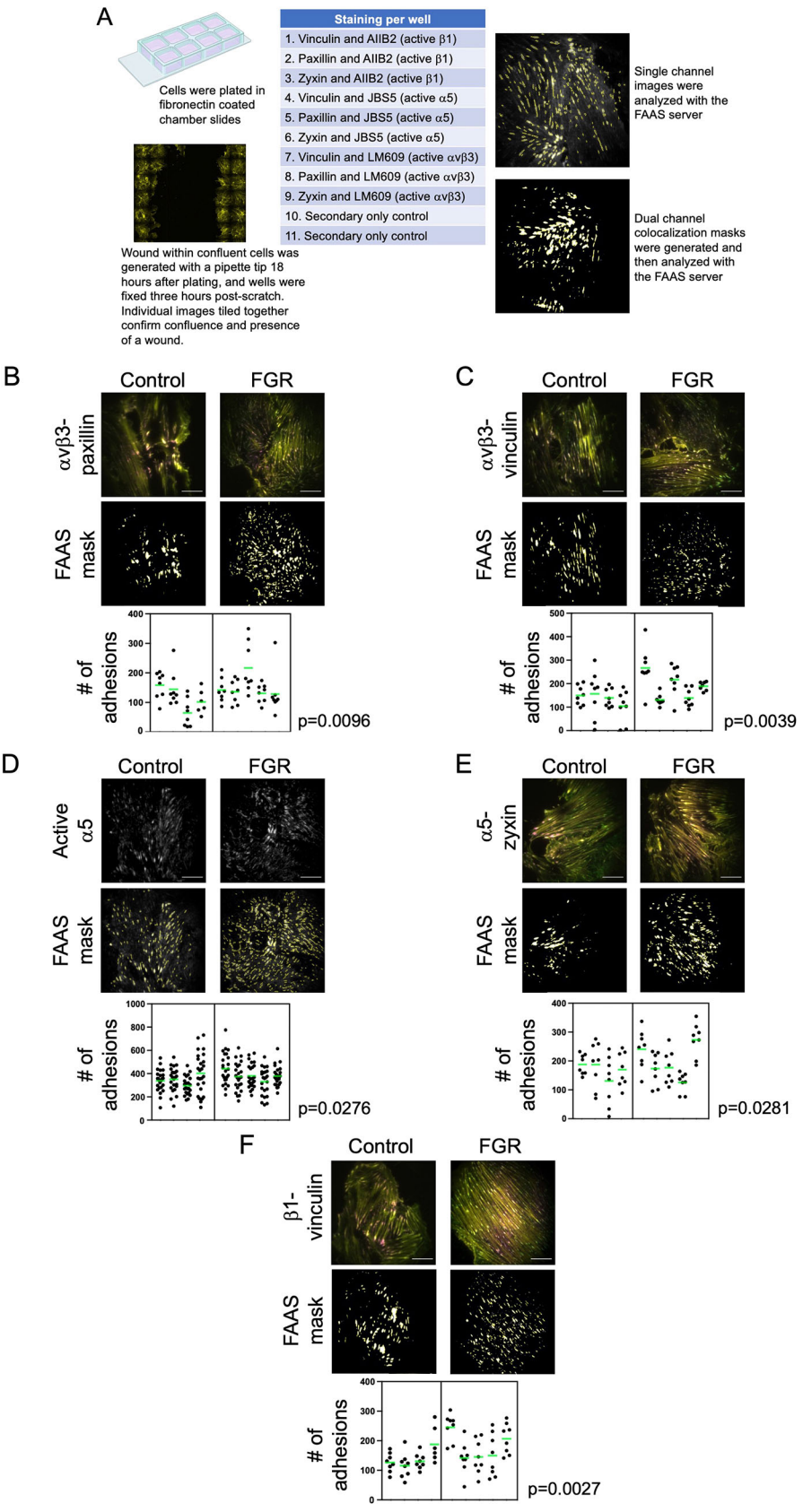

Fig. 5. Integrin α5β1 and αvβ3 focal adhesion complexes are altered in FGR endothelial cells. (A) Details of the experimental design using TIRF imaging followed by the Focal Adhesion Analysis Server (FAAS) for quantification. (B-F) Representative raw images and masks demonstrate significantly increased numbers of integrin αvβ3-paxillin (B; eight ROIs per subject, P=0.0096) and αvβ3-vinculin (C; eight ROIs per subject, P=0.0039). There were also significantly more numbers of active integrin a5 (D; 32 ROIs per subject, P=0.0276), α5-zyxin (E; eight ROIs per subject, P=0.0281) and β1-vinculin (F; eight ROIs per subject, P=0.0027). Three subjects (two control and one FGR) were removed from analysis due to positive fluorescent signal with secondary antibody only staining, with n=4 controls and n=5 FGR subjects. Green horizontal lines represent the mean for normally distributed data or median for non-normally distributed data. Unpaired two-tailed Student's t-tests were used for statistical comparisons when data were parametric (C-F), and Mann–Whitney U-tests were used for non-parametric data (B). Scale bars: 20 µm.

Second, crosstalk between integrins α5β1 and αvβ3 exists, and signaling redundancies introduce additional complexity (Benito-Jardón et al., 2017; Diaz et al., 2020; Holderfield and Hughes, 2008; Laurens et al., 2009; Samaržija et al., 2020). Interestingly, we investigated integrin α5 and β1 individually, and results for both subunits were not consistently uniform. For example, in FGR there appeared to be more active α5 within mature focal adhesions, but this was not true for active β1. This suggests that α5β1 is not the only

Development (2022) 149, dev200717. doi:10.1242/dev.200717

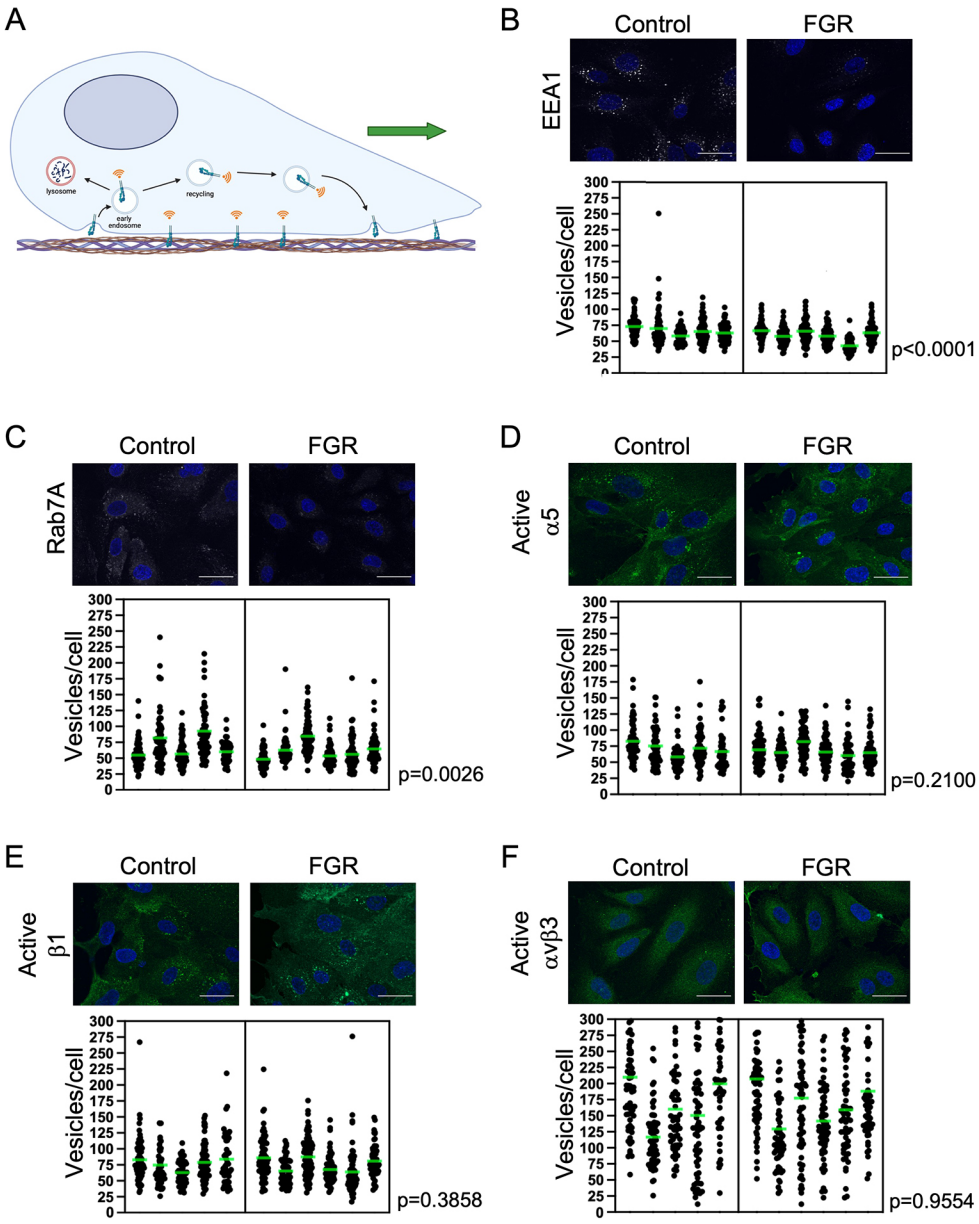

Fig. 6. Intracellular endosomal vesicles are reduced in FGR endothelial cells. (A) A graphical depiction of integrin intracellular trafficking during cell locomotion. (B,C) Representative images and graphical quantification demonstrate a significant reduction in early endosomes (B; EEA1, $P<0.0001$) and late endosomes (C; Rab7, $P=0.0026$) in FGR endothelial cells. (D-F) In contrast, representative images and quantification show similar amounts of internalized active integrin α5 (D), active integrin β1 (E) and active integrin αvβ3 (F) between control and FGR endothelial cells. $n=5$ controls and $n=6$ FGR subjects. One control subject was removed from analysis due to a high intensity secondary antibody threshold, which limited validation of the primary stain. At least 72 images containing 5-10 cells per image were analyzed per subject per stain. Green horizontal lines represent the mean for normally distributed data or median for non-normally distributed data. Unpaired two-tailed Student's *t*-tests were used for statistical comparisons when data were parametric (B,F), and Mann–Whitney *U*-tests were used for non-parametric data (C-E). Scale bars: 50 µm.

heterodimer that these two integrin subunits can form, which is supported by well-established studies demonstrating that integrin subunits are able to bind promiscuously and form alternate heterodimer combinations. These examples highlight the complexity of integrin regulation and are important considerations for future studies.

Beyond crosstalk and alternate heterodimer combinations, integrins α5β1and αvβ3 have also been shown to exhibit other regulatory features that were not comprehensively addressed with these experiments. One example is the role of α5β1 in fibronectin remodeling. In this situation, an extended integrin α5β1 heterodimer binds to fibronectin at the RGD (Asp-Gly-Arg) peptide sequence and provides the mechanical force to change the region from cyclical RGD repeats into a linear conformation, which, in turn, allows other α5β1and αvβ3 heterodimers to bind to the fibronectin RGD ligand (Benito-Jardón et al., 2017). In addition, this study does not investigate the downstream signaling effects that occur due to altered integrin regulation. These changes can include differences in signaling cascades both within the pathway used and aberrant localization of signal. Differences in signaling can result in changes to cytoskeletal organization, including cytoskeletal fibers such as actin, microtubules and intermediate filaments (Colello et al., 2012; DeMali et al., 2003; Hynes, 2002; Kramár et al., 2006; LaFlamme et al., 2018; Leube et al., 2015; Maniotis et al., 1997; Reverte et al., 2006). These downstream consequences of integrin regulation are also important factors in successful cell migration and need to be investigated.

It is also possible that our results, which were found in macrovascular endothelial cells isolated from the chorionic plate, may be different within microvascular endothelial cells of the placenta. We chose to use macrovascular placental endothelial cells isolated from the chorionic plate for two main reasons. First, our lab has previously established that these cells exhibit migratory defects, suggesting that they display angiogenic dysfunction. Second, proteomic analyses of control versus FGR human umbilical vein endothelial cells have shown that several proteins implicated in angiogenesis are altered in these macrovascular endothelial cells (Caniuguir et al., 2016). In contrast, we acknowledge that

Development (2022) 149, dev200717. doi:10.1242/dev.200717

microvascular fetoplacental endothelial cells have been shown to play a role in the formation of the placental vasculature (Sobrevia et al., 2011). These cells have been found to proliferate in greater quantities than umbilical vein endothelial cells in response to VEGF (Lang et al., 2003). Furthermore, microvascular endothelial cells essentially abut to syncytiotrophoblasts, the placental cells in direct contact with maternal blood, and therefore may be recipients of direct maternal or syncytiotrophoblastic signaling that could further affect angiogenic potential. Ultimately, it remains unknown whether a dysfunctional macrovasculature drives additional impairments in the microvasculature or whether this model best recapitulates placental angiogenesis. However, for the reasons noted above, we felt it was important to start with these well-characterized, macrovascular endothelial cells and, in future studies, we will investigate whether these altered mechanisms are similar in the microvasculature.

Lastly, another important consideration is the gestational age of the subjects in each cohort. Angiogenesis is not static throughout gestation, and the lack of preterm placentas is a limitation in our study. However, using placentas from appropriately grown, gestational age-matched fetuses that delivered preterm for some other etiology other than FGR also leads to other potential confounders. As one example, there is increasing data to suggest that placental pathology related to placental insufficiency may also be evident in many cases of spontaneous preterm birth of appropriately grown fetuses (Jaiman et al., 2022; Lien et al., 2021; Morgan et al., 2013; Romero et al., 2014; Visser et al., 2021). Furthermore, our previously published data suggest that gestational age does not significantly affect migratory properties of isolated placental endothelial cells.

In summary, having a complete characterization of the integrin dysregulation associated with FGR is crucial for improved understanding of the mechanistic etiologies underlying the FGR *in utero* environment that are responsible for persistently altered endothelial cellular processes. As these findings demonstrate inherent cellular adaptations that occur in placental endothelial cells in response to FGR, it is possible that other fetal cells respond similarly and also maintain cellular adaptations created in response to the *in utero* environment long after delivery. Therefore, understanding mechanistic adaptations in the placenta will not only elucidate antenatal processes resulting in FGR but may also shed light on how exposure to FGR causes long-term health risks, which will be invaluable if new preventative or treatment modalities are to be developed.

MATERIALS AND METHODS

Subject selection

The Colorado Multiple Institutional Review Board (COMIRB) approved all study protocols. Subjects from two groups were identified: (1) singleton pregnancies complicated by severe FGR as defined by an estimated fetal weight of less than the 10th percentile for gestational age and absent or reversed end-diastolic umbilical artery velocities, thereby necessitating delivery no later than 34 weeks gestation (range 24-34 weeks) (FGR); and (2) singleton pregnancies that resulted in full-term, appropriately grown fetuses delivered via cesarean section in the absence of labor (controls). All subjects, regardless of their categorization, were required to meet solid dating criteria as defined by the American College of Obstetricians and Gynecologists (ACOG Committee on Practice Bulletins – Obstetrics, 2017). Furthermore, pathologic growth restriction was confirmed postnatally by birthweight less than the 10th percentile for gestational age in the FGR cohort, whereas birthweight percentiles were all normal within the control group. Exclusion criteria for all groups consisted of any maternal use of tobacco, alcohol, cannabis or illicit drugs during pregnancy, conception as a result of *in vitro* fertilization, fetal anomaly, fetal aneuploidy, fetal or maternal infection and maternal morbidities including diabetes, history of thrombosis or antiphospholipid antibody syndrome. Eligible subjects were approached, and informed consent was obtained.

Placental endothelial cell isolation

Placental endothelial cells were isolated as previously described, with modifications (Jinga et al., 2000; Lang et al., 2003). Placentas were collected within 1 h of delivery and processed in a sterile tissue culture hood. To isolate fetoplacental macrovascular endothelial cells, the umbilical vein was cannulated with an IV catheter. Upon successful cannulation, sterile phosphate buffered saline (PBS) was injected into the vein and used to visualize vessels that branch off the umbilical vein. An arteriovenous (AV) fistula needle was then inserted into the distal end of the vessel. PBS was injected into the previously cannulated umbilical vein, and once PBS flow-through was visualized in the vessel and exiting the AV cannula, the vessel was considered properly perfused. Once this was established, digestive enzymes containing 0.1% (w/v) collagenase dispase (Roche Applied Science), 0.1% (w/v) bovine serum albumin (BSA) (Sigma-Aldrich), 0.2% (w/v) collagenase from clostridium (Sigma-Aldrich) and 1× antibiotic/antimycotic solution (Gibco) were added to the vessel. Enzymes were incubated within the vessel for 20 min at room temperature. After the incubation, an additional 50 ml of PBS was used to flush the vessel, and contents were collected. This cell suspension was centrifuged at 500 ***g*** for 10 min. The supernatant was removed, and the pellet was resuspended EGM-MV (Lonza) and plated on a 6 cm tissue-culture treated dish. After 24 h, the plate was washed twice gently with PBS and once with warm EGM-MV. At this time, the plate was inspected for attached endothelial colonies. Daily wash and media changes occurred for the first 3 days post isolation and then every other day thereafter. Following colony expansion, stock vials were frozen and kept in liquid nitrogen for long-term storage. Cell purity was established as previously published and, on the basis of this previous data, we determined that cells retained an endothelial phenotype up to the fifth passage and for these experiments only cells between passage 2 and 4 were used (Ji et al., 2021; Su et al., 2007). Contamination tests were performed every 3 months.

Scratch wound assay

IncuCyte ImageLock 96 well plates (Essen Biosciences) were coated with 10 µg/ml Fibronectin (Gibco), and plates were incubated at 4°C overnight. Coated plates were washed 2× with PBS before plating cells. Cells were seeded onto pre-coated plates the night before wound generation with 5.5×10^4 cells per well to achieve 100% confluence before scratch-wound generation. Cells were incubated overnight in EGM-MV (Lonza). Fully confluent wells were scratched using the WoundMaker (Essen Biosciences). Wells were washed 1× with PBS and 1× with warmed media. Fresh media containing treatment or isotype control conditions were added to each well (Table S1). Plates were placed in the IncuCyte (Sartorius) and imaged every 2 h for 24 h. IncuCyte software was used to segment images, generating image masks that allowed for the calculation of %RWD, which was calculated as the density of the wound at the specific time point minus the density of the wound at time zero divided by the density of the cell area at the specific time point minus the density of the wound at time zero. This calculation roughly accounts for potential differences in cell proliferation during the 24 h time period of the assay.

Quantitative real-time polymerase chain reaction (qRT-PCR)

Cells were plated in 6 cm tissue-culture treated plastic plates coated with 10 µg/ml fibronectin (Gibco) in 1× sterile PBS for 18 h before RNA isolation and were collected at 70-80% confluence. RNA was isolated using RNeasy micro kit (Qiagen). To determine RNA concentration and purity, NanoDrop (Thermo Fisher Scientific) spectrophotometric analysis was performed on each sample. cDNA synthesis was performed using qScript cDNA Supermix (Quantabio) in a SimpliAmp thermal cycler. qRT-PCR using SYBR green master mix (Applied Biosystems) was run in a QuantStudio 6 Flex Real Time PCR systems machine. *RPLP0* (36B4) was used as an internal reference gene and relative expression was calculated using the 2^−(ΔΔCT) method, where ΔCT is calculated as [mean CT(gene

Development (2022) 149, dev200717. doi:10.1242/dev.200717

of interest)−mean CT(reference gene)]. Mean CTs were generated from technical triplicates. ΔΔCT is calculated as [ΔCT(subject)−ΔCT(average of all control subjects)]. Relative expression for each subject is calculated as mean fold change which equals 2^−(ΔΔCT). Primer sequences are provided in Table S2. All primers were optimized and validated before use and were procured from Integrated DNA Technologies.

Western blot

Cells were plated in 6 cm tissue-culture treated plastic plates coated with 10 µg/ml fibronectin (Gibco) in 1× sterile PBS for 18 h before isolation and were harvested between 70-80% confluence. Cells were lysed in chilled mammalian protein extraction reagent (M-PER) lysis buffer (Thermo Fisher Scientific) containing 1X HALT protease/phosphatase inhibitor cocktail (Thermo Fisher Scientific). To ensure complete lysis, cells were placed on ice and vortexed for 30 s every 5 min over 20 min total. Lysed cells were then centrifuged at 18,407 ***g*** for 10 min at 4°C. Supernatant containing soluble proteins was removed and transferred to a fresh microcentrifuge tube, and the insoluble fraction was discarded. Protein concentration was determined using a Pierce BCA (Thermo Fisher Scientific) according to the manufacturer's instructions. Clarified lysates were prepared at a final concentration of 0.2 µg/µl in fluorescent master mix (ProteinSimple) and boiled for 5 min at 95°C. Samples, antibodies, blocking solution and protein normalization stain (ProteinSimple) were all added to the capillary electrophoresis plate (JESS, ProteinSimple). The plate and capillaries were then added to and imaged in the JESS machine. All analyses were completed using Compass software (ProteinSimple). Antibody information is provided in Table S3.

Isolation of integrin-based adhesions and complexes at the cell membrane

Isolation of integrin-based adhesions and complexes was adapted from a previously published protocol (Jones et al., 2015). Tissue-culture treated plates (10 cm) were coated with 10 µg/ml of fibronectin (Gibco) and incubated at 4°C overnight. Cells were seeded at a density of 1.0×10^6 per plate and incubated at 37°C for 2.5 h. After incubation, cells were cross-linked with 1.85 mg/ml dimethyl dithiobispropionimidate (DTBP) in serum-free Dulbecco's modified eagle medium (DMEM, Gibco) and incubated at 37°C for 5 min. Tris-HCl (1 M) was used to quench the DTBP cross-linking reaction and plates were washed with ice-cold PBS. Plates were pulse-sonicated with an ultrasonic cell homogenizer. Freshly prepared adhesion recovery solution [100 µl of 125 mM Tris-HCl (pH 6.8), 1% (w/v) SDS, 150 mM dithiothreitol (DTT) in ddH_2O] was then added to each plate. Complexes were collected using a cell scraper and transferred to a fresh microcentrifuge tube with 2× volume of acetone. Samples were precipitated at −80°C overnight. The next day samples were centrifuged at 16,000 ***g*** for 20 min at 4°C. The supernatant was removed ensuring that the precipitate remained intact. Fresh cold acetone (1 ml) was added, and samples were centrifuged again at 16,000 ***g*** for 20 min at 4°C. The supernatant was again removed, and sample precipitates were allowed to air dry for 20 min. After drying, 15 µl of MPER lysis buffer (Thermo Fisher Scientific) per plate was added to each tube of pooled sample and samples were heated at 70°C for 20 min, shaking at 1000 RPM. The protocol is represented in Fig. S4. Colorimetric protein concentration assays such as a Pierce BCA are not suitable for this sample preparation as adhesion recovery solution contains a high amount of DTT and residuals remain after acetone precipitation, rendering protein concentration interpretations unreliable. Therefore, the same volume of sample was loaded across all subjects in place of loading the same concentration of protein. JESS ProteinSimple was used for immunoblot analyses, which allowed us to incorporate a protein normalization standard that has been shown to be at least equivalent to traditional housekeeping proteins. Antibody information for analysis of integrin-based adhesion complexes at the membrane is provided in Table S4.

Immunofluorescence

Cells were seeded on either glass bottom chamber slides (Ibidi) or glass coverslips coated with 10 µg/ml fibronectin (Gibco). Immunofluorescence staining was performed on cells fixed with 4% paraformaldehyde for 20 min at room temperature. If only membrane-bound proteins were examined, fixed cells were not permeabilized; otherwise, cells were permeabilized with 3% Triton X-100 in PBS for 10 min on a shaking platform at room temperature. After washing, cells were blocked in 2.0% BSA in 0.1% Triton X-100 for 1 h and incubated with primary antibody with previously optimized concentrations (Tables S5 and S6) shaking overnight at 4°C. The following day, cells were washed and incubated with secondary antibody with previously optimized concentrations (Tables S5 and S6) for 1 h shaking at room temperature in a light-impermeable box. For images requiring actin analysis, cells were treated with Phalloidin-Alexa 594 (1:5000, Invitrogen) for 15 min in PBS. DAPI was used to stain nuclei (Invitrogen NucBlue-R37606): two drops per milliliter for 5 min in PBS. Stained cells remained in PBS and were immediately imaged. Stained cells were imaged via confocal microscopy using the Olympus FV1000 or the Zeiss Elyra P1 for TIRF microscopy. Any subjects displaying fluorescent signal in secondary only controls were removed from further analyses. The investigators acquiring all microscopy images were blinded to subject group during the entirety of the experiment (cell culture through image analysis).

Image analysis

To quantify the amount of active versus total integrin present at the cell surface, FIJI was used to determine the fluorescence signal in each channel and the active integrin stain intensity was divided by the total stain intensity, thereby generating an intensity ratio. Three-channel TIRF focal adhesion images were separated into single channel grayscale images of focal adhesion and active integrin markers, converted to stacked TIFF images with FIJI, and sent to the open access Focal Adhesion Analysis Server (FAAS) (Berginski and Gomez, 2013) for automated analysis of the number of focal adhesions per image. Currently, FAAS only has the capability to process single channel images. Therefore, to analyze co-stained images, binary colocalization masks were generated with the colocalization image creator FIJI plugin (Lunde and Glover, 2020) and then sent to FAAS. All output images generated by FAAS were manually inspected to ensure accuracy.

To quantify the endosomes stained with an endocytic vesicle marker or an active integrin, FIJI plugins were used to count the number of DAPI-positive nuclei and the number of vesicles per cell. The number of vesicles were divided by the total number of DAPI-positive nuclei to generate the number of vesicles per cell.

Statistical analysis

Clinical characteristics between control and FGR subjects were compared using two-tailed paired *t*-tests after confirmation of normally distributed datasets by the Shapiro-Wilk test for normality. The Mann–Whitney *U*-test was used for non-parametric data, and Fisher's exact test was used for categorical data. All cellular experiments used cells between the second and fourth passage. Representative images of experiments are from one subject per group, with analysis of numerical results and graphical representation accounting for all subjects. Numerical data are reported as means of the replicates performed within all subjects, with error bars representing s.e.m. After determining parametric or non-parametric distribution, two-tailed unpaired *t*-tests or Mann–Whitney *U*-tests were used to compare differences between FGR and control cells for all experiments except the scratch wound assay. For *t*-tests and *U*-tests, a value of $P<0.05$ was considered significant. For scratch wound assays, the percent relative wound density was calculated and plotted over time. A non-linear regression fitted for a sigmoidal curve was used to compare differences in migratory capacity. For these more sensitive statistical tests, a value of $P<0.01$ was considered significant.

Acknowledgements

We are grateful to the Perinatal Research Core for identifying, approaching and consenting eligible subjects. The University of Colorado Cancer Center Cell Technologies Shared Resource was a great help with IncuCyte migration assays. The imaging experiments were performed in the Advanced Light Microscopy Core as part of the NeuroTechnology Center at the University of Colorado Anschutz Medical Campus supported in part by the Rocky Mountain Neurological Disorders Core (P30 NS048154) and the Diabetes Research Center (P30 DK116073).

Competing interests
The authors declare no competing or financial interests.

Author contributions
Conceptualization: D.L.G., E.J.S.; Methodology: D.L.G., A.F., K.M., D.S., R.M.; Formal analysis: D.L.G.; Investigation: D.L.G., S.J.; Resources: E.J.S.; Data curation: D.L.G.; Writing - original draft: D.L.G.; Writing - review & editing: S.J., D.S., R.M., E.J.S.; Visualization: D.L.G., S.J., D.S., R.M.; Supervision: E.J.S.; Project administration: E.J.S.; Funding acquisition: E.J.S.

Funding
This work was supported by the National Institutes of Health (HL119846 to E.J.S.). Deposited in PMC for release after 12 months.

Peer review history
The peer review history is available online at https://journals.biologists.com/dev/lookup/doi/10.1242/dev.200717.reviewer-comments.pdf.

References

ACOG Committee on Practice Bulletins—Obstetrics (2017). Committee Opinion No 700. *Obstet. Gynecol.* **129**, e150-e154. doi:10.1097/AOG.0000000000002046

Alfirevic, Z., Stampalija, T. and Dowswell, T. (2017). Fetal and umbilical Doppler ultrasound in high-risk pregnancies. *Cochrane database Syst. Rev.* **6**, CD007529 doi:10.1002/14651858.CD007529.pub4

Balcioglu, H. E., van de Water, B. and Danen, E. H. J. (2016). Tumor-induced remote ECM network orientation steers angiogenesis. *Sci. Rep.* **6**, 22580. doi:10.1038/srep22580

Baschat, A. A., Gembruch, U., Reiss, I., Gortner, L., Weiner, C. P. and Harman, C. R. (2000). Relationship between arterial and venous Doppler and perinatal outcome in fetal growth restriction. *Ultrasound Obstet. Gynecol.* **16**, 407-413. doi:10.1046/j.1469-0705.2000.00284.x

Baschat, A. A., Gembruch, U. and Harman, C. R. (2001). The sequence of changes in Doppler and biophysical parameters as severe fetal growth restriction worsens. *Ultrasound Obstet. Gynecol.* **18**, 571-577. doi:10.1046/j.0960-7692.2001.00591.x

Benito-Jardón, M., Klapproth, S., Gimeno-LLuch, I., Petzold, T., Bharadwaj, M., Müller, D. J., Zuchtriegel, G., Reichel, C. A. and Costell, M. (2017). The fibronectin synergy site re-enforces cell adhesion and mediates a crosstalk between integrin classes. *eLife* **6**, e22264. doi:10.7554/eLife.22264

Berginski, M. E. and Gomez, S. M. (2013). The Focal Adhesion Analysis Server: a web tool for analyzing focal adhesion dynamics. *F1000Research* **2**, 68. doi:10.12688/f1000research.2-68.v1

Byzova, T. V., Rabbani, R., D'Souza, S. E. and Plow, E. F. (1998). Role of integrin alpha(v)beta3 in vascular biology. *Thromb. Haemost.* **80**, 726-734. doi:10.1055/s-0037-1615250

Caniuguir, A., Krause, B. J., Hernandez, C., Uauy, R. and Casanello, P. (2016). Markers of early endothelial dysfunction in intrauterine growth restriction-derived human umbilical vein endothelial cells revealed by 2D-DIGE and mass spectrometry analyses. *Placenta* **41**, 14-26. doi:10.1016/j.placenta.2016.02.016

Chen, C. P. and Aplin, J. D. (2003). Placental extracellular matrix: gene expression, deposition by placental fibroblasts and the effect of oxygen. *Placenta* **24**, 316-325. doi:10.1053/plac.2002.0904

Clark, R. A., Tonnesen, M. G., Gailit, J. and Cheresh, D. A. (1996). Transient functional expression of alphaVbeta 3 on vascular cells during wound repair. *Am. J. Pathol.* **148**, 1407-1421.

Colello, D., Mathew, S., Ward, R., Pumiglia, K. and LaFlamme, S. E. (2012). Integrins regulate microtubule nucleating activity of centrosome through mitogen-activated protein kinase/extracellular signal-regulated kinase kinase/extracellular signal-regulated kinase (MEK/ERK) signaling. *J. Biol. Chem.* **287**, 2520-2530. doi:10.1074/jbc.M111.254128

Crimmins, S., Desai, A., Block-Abraham, D., Berg, C., Gembruch, U. and Baschat, A. A. (2014). A comparison of Doppler and biophysical findings between liveborn and stillborn growth-restricted fetuses. *Am. J. Obstet. Gynecol.* **211**, 669.e1-669.e10. doi:10.1016/j.ajog.2014.06.022

De Palma, M., Biziato, D. and Petrova, T. V. (2017). Microenvironmental regulation of tumour angiogenesis. *Nat. Rev. Cancer* **17**, 457-474. doi:10.1038/nrc.2017.51

DeMali, K. A., Wennerberg, K. and Burridge, K. (2003). Integrin signaling to the actin cytoskeleton. *Curr. Opin. Cell Biol.* **15**, 572-582. doi:10.1016/S0955-0674(03)00109-1

Diaz, C., Neubauer, S., Rechenmacher, F., Kessler, H. and Missirlis, D. (2020). Recruitment of $\alpha_v\beta_3$ integrin to $\alpha_5\beta_1$ integrin-induced clusters enables focal adhesion maturation and cell spreading. *J. Cell Sci.* **133**, jcs232702. doi:10.1242/jcs.232702

Gordijn, S. J., Beune, I. M., Thilaganathan, B., Papageorghiou, A., Baschat, A. A., Baker, P. N., Silver, R. M., Wynia, K. and Ganzevoort, W. (2016). Consensus definition of fetal growth restriction: a Delphi procedure. *Ultrasound Obstet. Gynecol.* **48**, 333-339. doi:10.1002/uog.15884

Holderfield, M. T. and Hughes, C. C. W. (2008). Crosstalk between vascular endothelial growth factor, notch, and transforming growth factor-beta in vascular morphogenesis. *Circ. Res.* **102**, 637-652. doi:10.1161/CIRCRESAHA.107.167171

Hynes, R. O. (2002). Integrins: bidirectional, allosteric signaling machines. *Cell* **110**, 673-687. doi:10.1016/S0092-8674(02)00971-6

Jackson, M. R., Walsh, A. J., Morrow, R. J., Mullen, J. B. M., Lye, S. J. and Ritchie, J. W. (1995). Reduced placental villous tree elaboration in small-for-gestational-age pregnancies: relationship with umbilical artery Doppler waveforms. *Am. J. Obstet. Gynecol.* **172**, 518-525. doi:10.1016/0002-9378(95)90566-9

Jaiman, S., Romero, R., Bhatti, G., Jung, E., Gotsch, F., Suksai, M., Gallo, D. M., Chaiworapongsa, T. and Kadar, N. (2022). The role of the placenta in spontaneous preterm labor and delivery with intact membranes. *J. Perinat. Med.* **50**, 553-566. doi:10.1515/jpm-2021-0681

Ji, S., Xin, H. and Su, E. J. (2019). Overexpression of the aryl hydrocarbon receptor nuclear translocator partially rescues fetoplacental angiogenesis in severe fetal growth restriction. *Clin. Sci.* **133**, 1353-1365. doi:10.1042/CS20190381

Ji, S., Gumina, D., McPeak, K., Moldovan, R., Post, M. D. and Su, E. J. (2021). Human placental villous stromal extracellular matrix regulates fetoplacental angiogenesis in severe fetal growth restriction. *Clin. Sci.* **135**, 1127-1143. doi:10.1042/CS20201533

Jinga, V. V., Gafencu, A., Antohe, F., Constantinescu, E., Heltianu, C., Raicu, M., Manolescu, I., Hunziker, W. and Simionescu, M. (2000). Establishment of a pure vascular endothelial cell line from human placenta. *Placenta* **21**, 325-336. doi:10.1053/plac.1999.0492

Jones, M. C., Humphries, J. D., Byron, A., Millon-Frémillon, A., Robertson, J., Paul, N. R., Ng, D. H. J., Askari, J. A. and Humphries, M. J. (2015). Isolation of integrin-based adhesion complexes. *Curr. Protoc. Cell Biol.* 66, 9.8.1-9.8.15. doi:10.1002/0471143030.cb0908s66

Kramár, E. A., Lin, B., Rex, C. S., Gall, C. M. and Lynch, G. (2006). Integrin-driven actin polymerization consolidates long-term potentiation. *Proc. Natl. Acad. Sci. USA* **103**, 5579-5584. doi:10.1073/pnas.0601354103

Krebs, C., Macara, L. M., Leiser, R., Bowman, A. W., Greer, I. A. and Kingdom, J. C. P. (1996). Intrauterine growth restriction with absent end-diastolic flow velocity in the umbilical artery is associated with maldevelopment of the placental terminal villous tree. *Am. J. Obstet. Gynecol.* **175**, 1534-1542. doi:10.1016/S0002-9378(96)70103-5

LaFlamme, S. E., Mathew-Steiner, S., Singh, N., Colello-Borges, D. and Nieves, B. (2018). Integrin and microtubule crosstalk in the regulation of cellular processes. *Cell. Mol. Life Sci.* **75**, 4177-4185. doi:10.1007/s00018-018-2913-x

Lang, I., Pabst, M. A., Hiden, U., Blaschitz, A., Dohr, G. and Hahn, T. (2003). Heterogeneity of microvascular endothelial cells isolated from human term placenta and macrovascular umbilical vein endothelial cells. *Eur. J. Cell Biol.* **82**, 163-173. doi:10.1078/0171-9335-00306

Laurens, N., Engelse, M. A., Jungerius, C., Löwik, C. W., van Hinsbergh, V. W. M. and Koolwijk, P. (2009). Single and combined effects of $\alpha v\beta 3$- and $\alpha 5\beta 1$-integrins on capillary tube formation in a human fibrinous matrix. *Angiogenes* **12**, 275-285. doi:10.1007/s10456-009-9150-8

Leube, R. E., Moch, M. and Windoffer, R. (2015). Intermediate filaments and the regulation of focal adhesion. *Curr. Opin. Cell Biol.* **32**, 13-20. doi:10.1016/j.ceb.2014.09.011

Lien, Y.-C., Zhang, Z., Cheng, Y., Polyak, E., Sillers, L., Falk, M. J., Ischiropoulos, H., Parry, S. and Simmons, R. A. (2021). Human placental transcriptome reveals critical alterations in inflammation and energy metabolism with fetal sex differences in spontaneous preterm birth. *Int. J. Mol. Sci.* **22**, 7899. doi:10.3390/ijms22157899

Lunde, A. and Glover, J. C. (2020). A versatile toolbox for semi-automatic cell-by-cell object-based colocalization analysis. *Sci. Rep.* **10**, 19027. doi:10.1038/s41598-020-75835-7

Maniotis, A. J., Chen, C. S. and Ingber, D. E. (1997). Demonstration of mechanical connections between integrins, cytoskeletal filaments, and nucleoplasm that stabilize nuclearstructure. *Proc. Natl. Acad. Sci. USA* **94**, 849-854. doi:10.1073/pnas.94.3.849

Martins, J. G., Biggio, J. R. and Abuhamad, A. (2020). Society for Maternal-Fetal Medicine Consult Series #52: Diagnosis and management of fetal growth restriction: (Replaces Clinical Guideline Number 3, April 2012). *Am. J. Obstet. Gynecol.* **223**, B2-B17. doi:10.1016/j.ajog.2020.05.010

Morgan, T. K., Tolosa, J. E., Mele, L., Wapner, R. J., Spong, C. Y., Sorokin, Y., Dudley, D. J., Peaceman, A. M., Mercer, B. M., Thorp, J. M. et al. (2013). Placental villous hypermaturation is associated with idiopathic preterm birth. *J. Matern. Fetal. Neonatal Med.* **26**, 647-653. doi:10.3109/14767058.2012.746297

Nicolaides, K. H., Bilardo, C. M., Soothill, P. W. and Campbell, S. (1988). Absence of end diastolic frequencies in umbilical artery: a sign of fetal hypoxia and acidosis. *Br. Med. J.* **297**, 1026-1027. doi:10.1136/bmj.297.6655.1026

Pardi, G., Cetin, I., Marconi, A. M., Lanfranchi, A., Bozzetti, P., Farrazzi, E., Buscaglia, M. and Battaglia, F. C. (2010). Diagnostic value of blood sampling in

fetuses with growth retardation. *N. Engl. J. Med.* **328**, 692-696. doi:10.1056/NEJM199303113281004

Pisaneschi, S., Boldrini, A., Genazzani, A. R., Coceani, F. and Simoncini, T. (2013). Feto-placental vascular dysfunction as a prenatal determinant of adult cardiovascular disease. *Intern. Emerg. Med.* **8** Suppl. 1, S41-S45. doi:10.1007/s11739-013-0925-y

Reverte, C. G., Benware, A., Jones, C. W. and LaFlamme, S. E. (2006). Perturbing integrin function inhibits microtubule growth from centrosomes, spindle assembly, and cytokinesis. *J. Cell Biol.* **174**, 491-497. doi:10.1083/jcb.200603069

Romero, R., Dey, S. K. and Fisher, S. J. (2014). Preterm labor: one syndrome, many causes. *Science* **345**, 760-765. doi:10.1126/science.1251816

Rüegg, C. and Mariotti, A. (2003). Vascular integrins: pleiotropic adhesion and signaling molecules in vascular homeostasis and angiogenesis. *Cell. Mol. Life Sci.* **60**, 1135-1157. doi:10.1007/s00018-003-2297-3

Sağol, S., Sağol, O. and Özdemir, N. (2002). Stereological quantification of placental villus vascularization and its relation to umbilical artery Doppler flow in intrauterine growth restriction. *Prenat. Diagn.* **22**, 398-403. doi:10.1002/pd.323

Salafia, C. M., Pezzullo, J. C., Minior, V. K. and Divon, M. Y. (1997). Placental pathology of absent and reversed end-diastolic flow in growth-restricted fetuses. *Obs. Gynecol* **90**, 830-836. doi:10.1016/S0029-7844(97)00473-0

Samaržija, I., Dekanić, A., Humphries, J. D., Paradžik, M., Stojanović, N., Humphries, M. J. and Ambriović-Ristov, A. (2020). Integrin crosstalk contributes to the complexity of signalling and unpredictable cancer cell fates. *Cancers (Basel).* **12**, 1910. doi:10.3390/cancers12071910

Sankaran, S. (2012). Creasy and Resnik's maternal–fetal medicine: principles and practice sixth edition. *Obstet. Med.* **5**, 88-89. doi:10.1258/om.2011.11E005

Sobrevia, L., Abarzúa, F., Nien, J. K., Salomón, C., Westermeier, F., Puebla, C., Cifuentes, F., Guzmán-Gutiérrez, E., Leiva, A. and Casanello, P. (2011). Review: Differential placental macrovascular and microvascular endothelial dysfunction in gestational diabetes. *Placenta* **32** Suppl. 2, S159-S164. doi:10.1016/j.placenta.2010.12.011

Su, E. J., Cheng, Y.-H., Chatterton, R. T., Lin, Z.-H., Yin, P., Reierstad, S., Innes, J. and Bulun, S. E. (2007). Regulation of 17-beta hydroxysteroid dehydrogenase type 2 in human placental endothelial cells1. *Biol. Reprod.* **77**, 517-525. doi:10.1095/biolreprod.106.059451

Su, E. J., Xin, H., Yin, P., Dyson, M., Coon, J., Farrow, K. N., Mestan, K. K. and Ernst, L. M. (2015). Impaired fetoplacental angiogenesis in growth-restricted fetuses with abnormal umbilical artery Doppler velocimetry is mediated by Aryl Hydrocarbon Receptor Nuclear Translocator (ARNT). *J. Clin. Endocrinol. Metab.* **100**, E30-E40. doi:10.1210/jc.2014-2385

Thornton, J. G., Hornbuckle, J., Vail, A., Spiegelhalter, D. J., Levene, M., Van Bulck, B., Kalakoutis, G. M., Kralove, H., Sak, P., Schneider, K. T. M. et al. (2004). Infant wellbeing at 2 years of age in the Growth Restriction Intervention Trial (GRIT): multicentred randomised controlled trial. *Lancet* **364**, 513-520. doi:10.1016/S0140-6736(04)16809-8

Todros, T., Piccoli, E., Rolfo, A., Cardaropoli, S., Guiot, C., Gaglioti, P., Oberto, M., Vasario, E. and Caniggia, I. (2011). Review: Feto-placental vascularization: a multifaceted approach. *Placenta* **32** Suppl. 2, S165-S169. doi:10.1016/j.placenta.2010.12.020

Visser, L., van Buggenum, H., van der Voorn, J. P., Heestermans, L. A. P. H., Hollander, K. W. P., Wouters, M. G. A. J., de Groot, C. J. M. and de Boer, M. A. (2021). Maternal vascular malperfusion in spontaneous preterm birth placentas related to clinical outcome of subsequent pregnancy. *J. Matern. Fetal. Neonatal Med.* **34**, 2759-2764. doi:10.1080/14767058.2019.1670811

Zhou, X., Rowe, R. G., Hiraoka, N., George, J. P., Wirtz, D., Mosher, D. F., Virtanen, I., Chernousov, M. A. and Weiss, S. J. (2008). Fibronectin fibrillogenesis regulates three-dimensional neovessel formation. *Genes Dev.* **22**, 1231-1243. doi:10.1101/gad.1643308

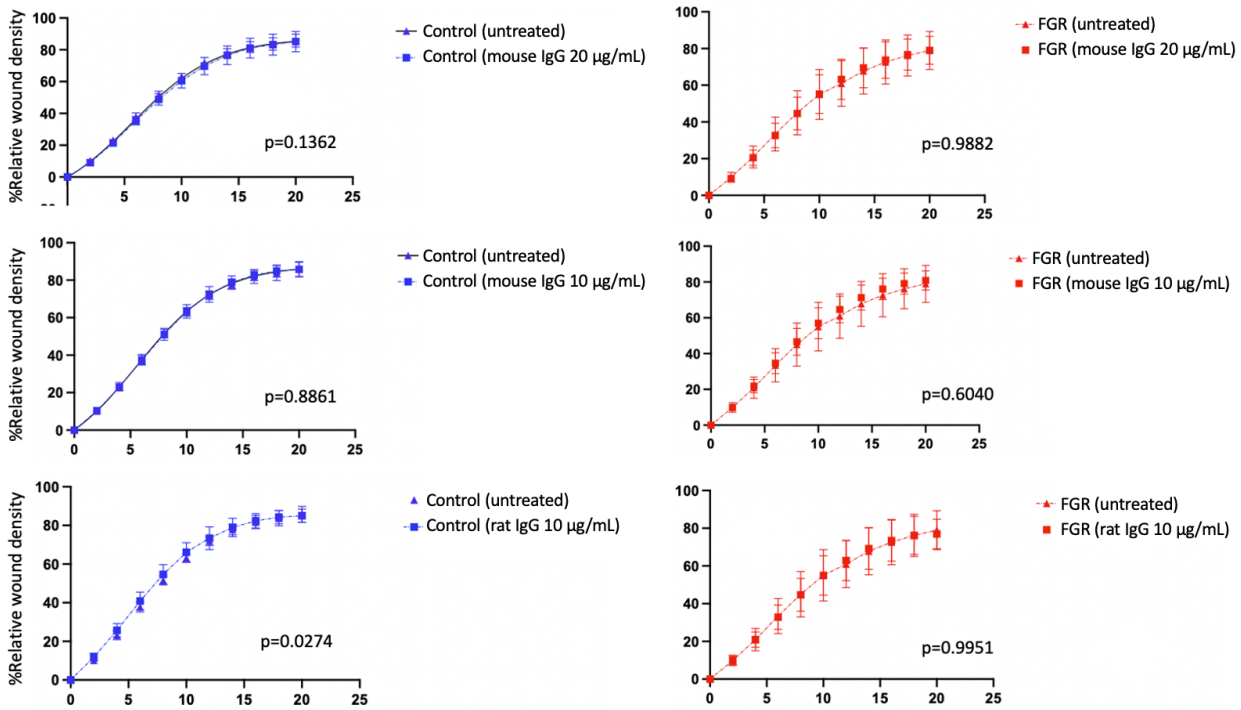

Fig. S1. There were no significant differences in migration when comparing untreated control and FGR endothelial cells to those treated with IgG isotype controls. All cells were plated on fibronectin (n=6 per group).

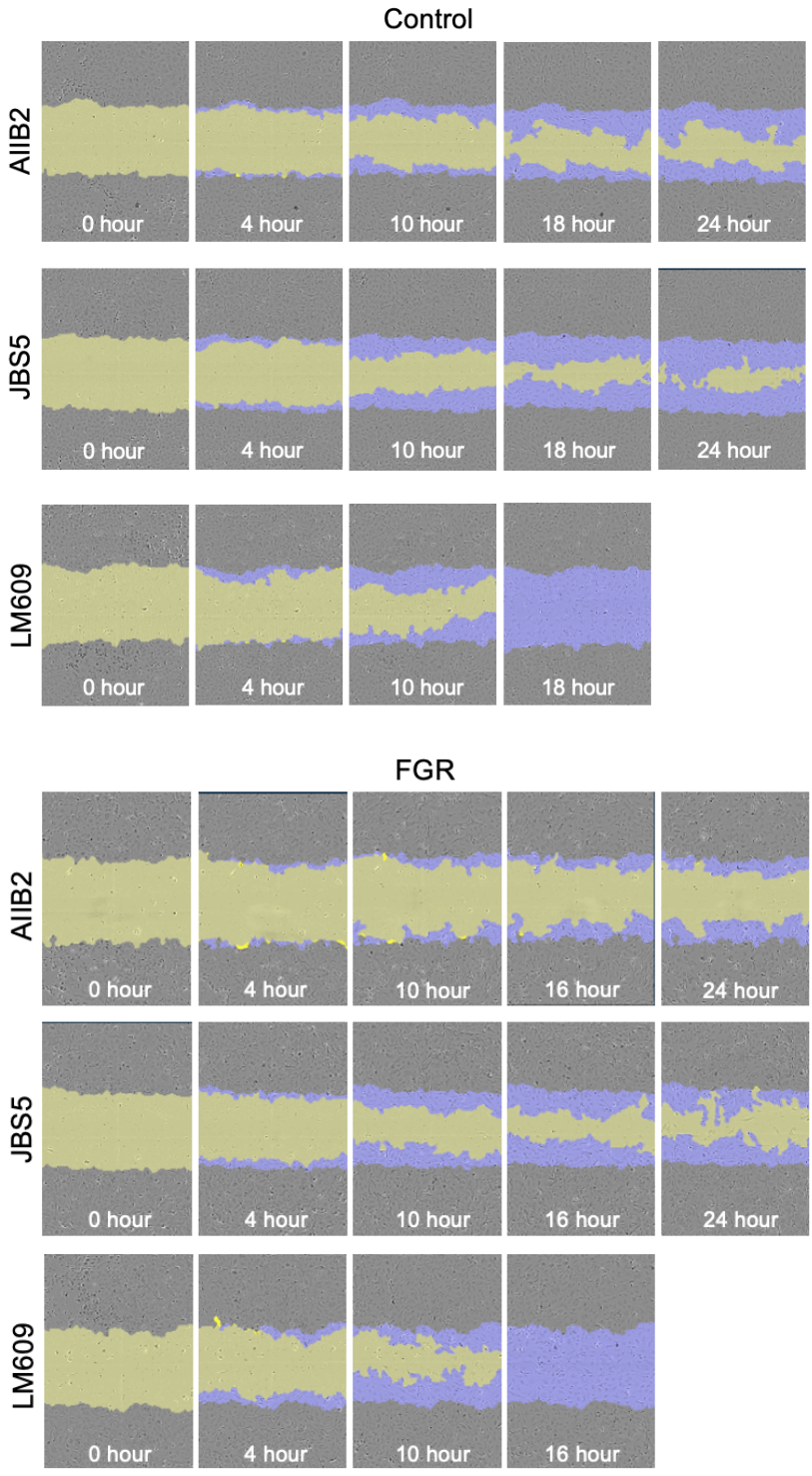

Fig. S2. Representative images of cell migration into the scratch wound and the masks used to generate %RWD for all treatment conditions in each cohort.

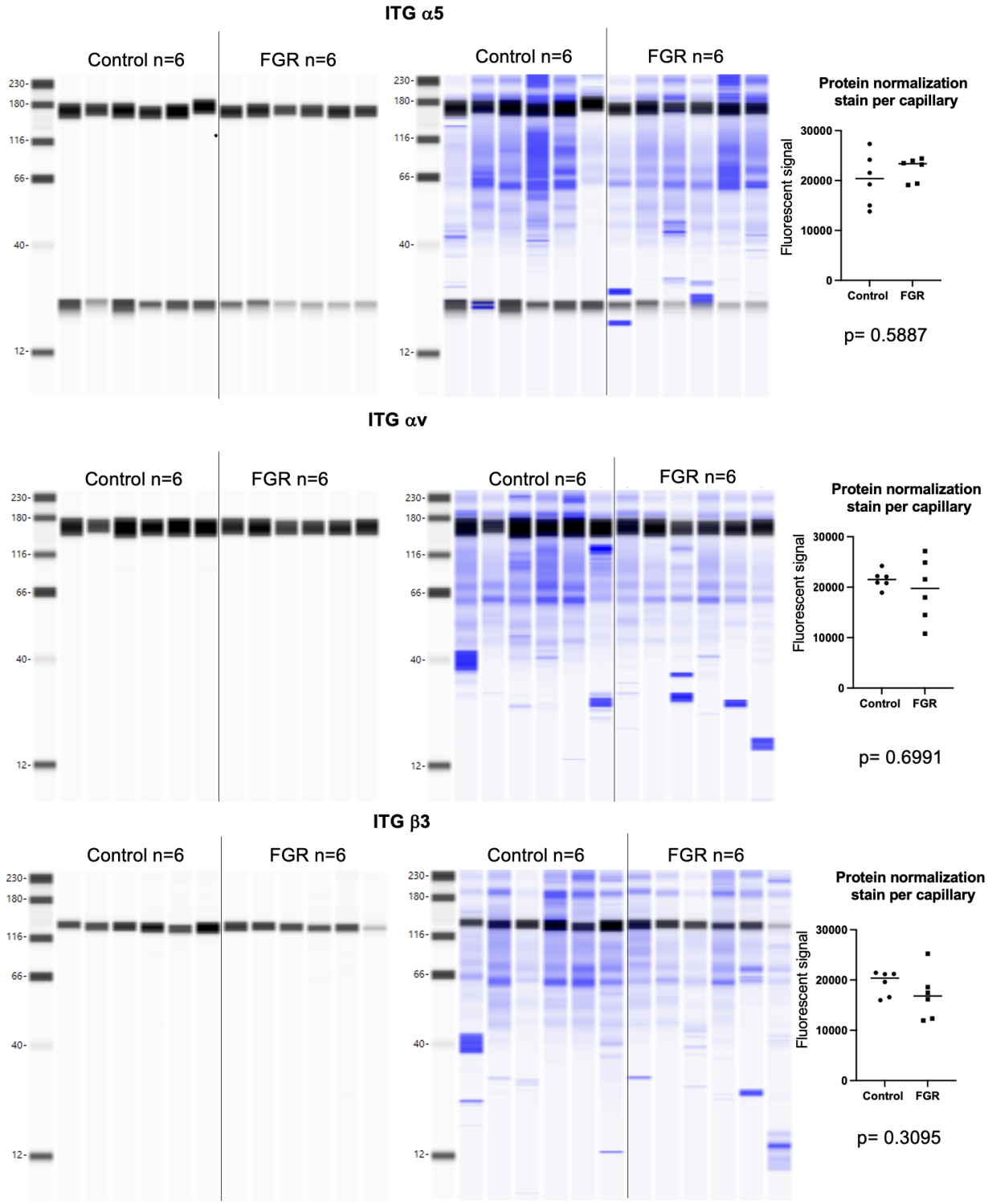

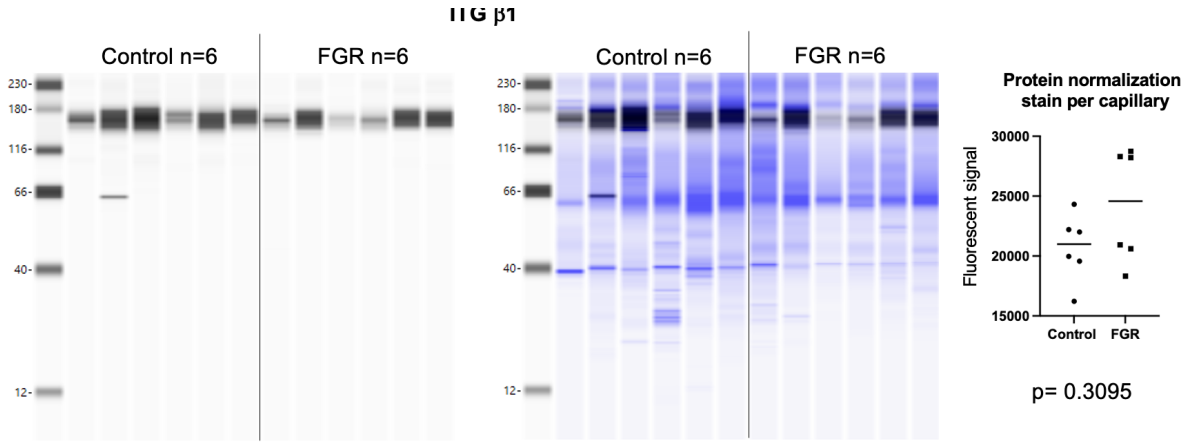

Fig. S3. Uncropped images of the immunoblots presented in Figure 3. The fluorescent signals in each group generated by the protein normalization stain (shown in blue) were compared with a Mann-Whitney U-test and showed no significant difference in protein normalization stain.

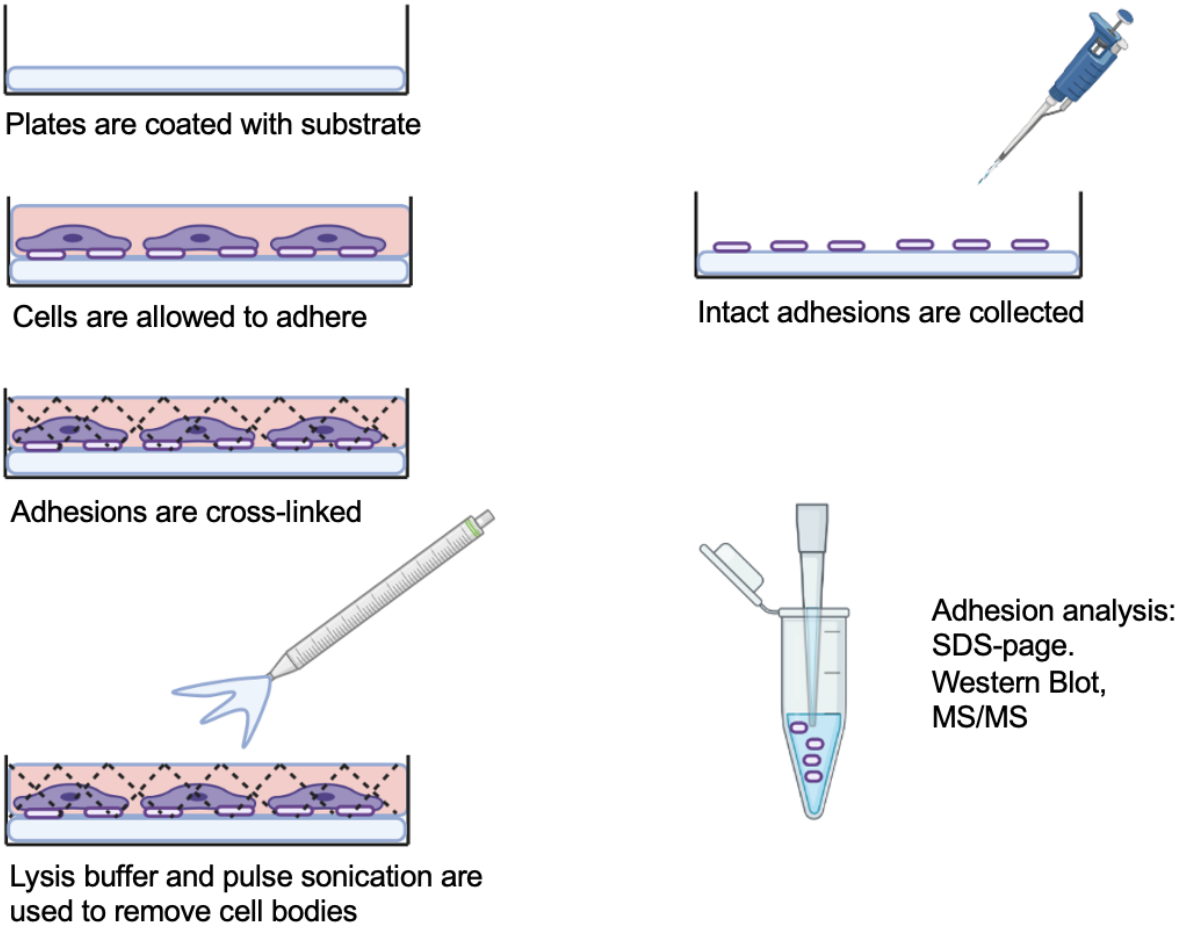

Fig. S4. Graphical depiction of the method used to isolate membrane focal adhesion complexes.

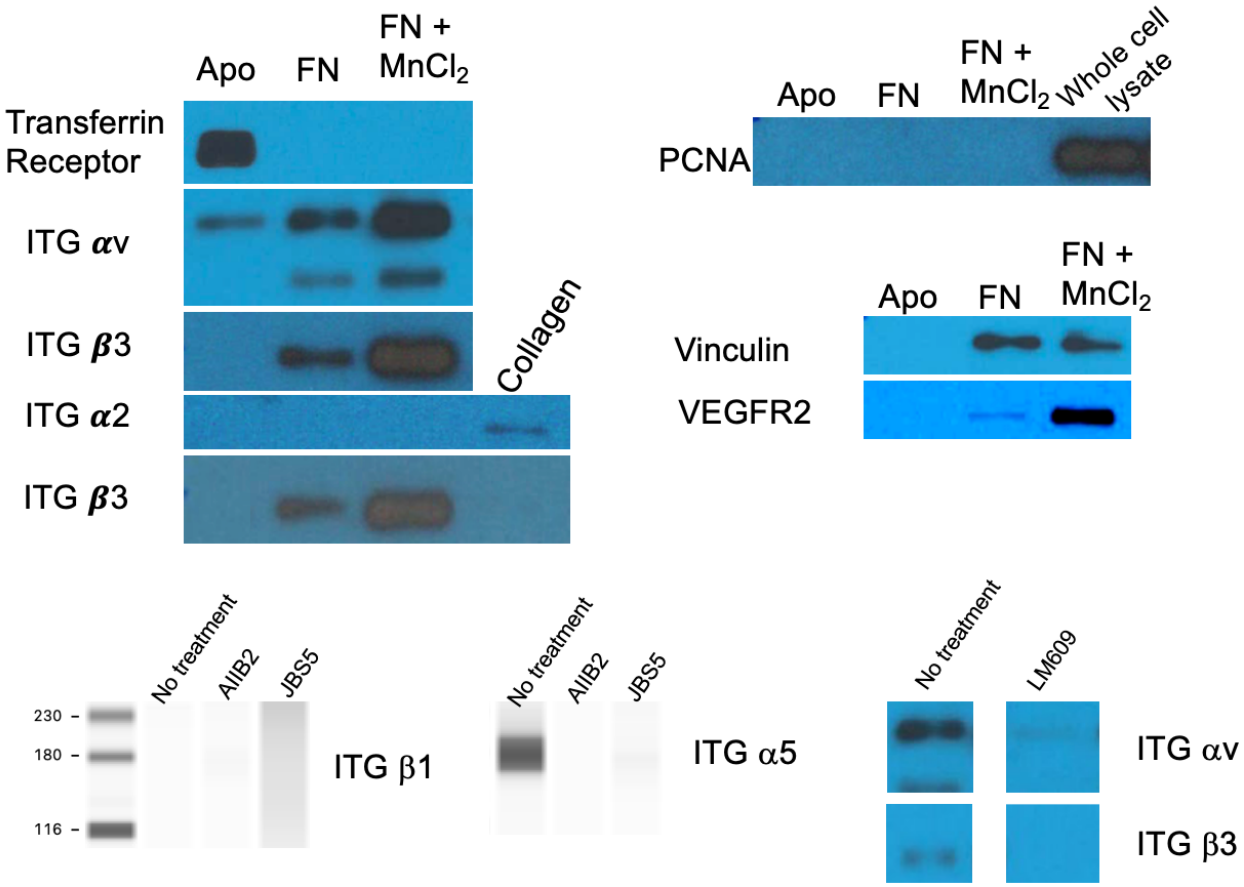

Fig. S5. Western Blot analysis for proof-of-concept experiments. Membranes were probed for either transferrin receptor, integrin av, b3, a2, PCNA, vinculin, or VEGFR2. Each sample was plated on a different substrate: Apotransferrin (Apo), fibronectin (FN), fibronectin + 1 mM $MnCl_2$ (FN+$MnCl_2$), collagen, and collagen + 1 mM $MnCl_2$ (Collagen+$MnCl_2$). Whole cell lysate was included as a positive control for PCNA as it should not be found in any isolates. In the lower panel, we show that when cells are treated with blocking antibodies (AIIB2, JBS5, and LM609), the corresponding integrins are inhibited from binding to fibronectin and are therefore not seen in isolates. Integrin b1 was not detectable in the no treatment condition. Proof-of-concept experiments were completed using 3 control subjects, and the experiment for each subject was repeated in triplicate.

Table S1. Antibodies and isotype controls utilized in the scratch wound assay.

Antibody Name	Species	Company Name/ Cat. No.	Application	Concentration used
AIIB2	Rat	DSHB University of Iowa	Blocking antibody - active Integrin β1	10 μg/mL
JBS5	Mouse	Santa Cruz/ sc-59762	Blocking antibody - active Integrin α5	10 μg/mL
LM609	Mouse	Abcam/ ab190147	Blocking antibody - active Integrin αvβ3	20 μg/mL
IgG1	Rat	Novus/ MAB005	Isotype control	10 μg/mL
IgG1	Mouse	Cell Signaling Technology/ #5415	Isotype control	10 μg/mL and 20 μg/mL

Table S2. Primer sequences.

Gene	Forward	Reverse
ITG AV	AGAATCAAGGAGAAGGTGCC	GGCGAGTTTGGTTTTCTGTC
ITG A5	GGCTCCTTCTTCGGATTCTC	TGCAAGGACTTGTACTCCAC
ITG B1	AATTAGGCCTCTGGGCTTTAC	GACGCACTCTCCATTGTTACT
ITG B3	CAGGCATTGTCCAGCCTAAT	CAGGTGGCATTGAAGGATAGAG
36B4	GCAGACAACGTGGGCTCCAAGCAGAT	GGTCCTCCTTGGTGAACACGAAGCCC

Table S3. Primary and secondary antibodies used for immunoblot analysis of whole endothelial cell lysate. All secondaries were conjugated with horseradish peroxidase.

Primary Antibody	Species	Company/ Cat. No.	Dilution	Secondary Antibody	Species	Company/Cat. No.
ITG αv	Rabbit	Abcam/ ab179475	1:500	anti-rabbit IgG	Goat	ProteinSimple/ DM-001
ITG α5	Rabbit	Abcam/ ab150361	1:500	anti-rabbit IgG	Goat	ProteinSimple/ DM-001
ITG β3	Rabbit	Abcam/ ab179473	1:200	anti-rabbit IgG	Goat	ProteinSimple/ DM-001
ITG β1	Mouse	Thermo/ 14-0299-82	1:100	anti-mouse IgG	Goat	ProteinSimple/ DM-002

Table S4. Primary and secondary antibodies used for immunoblot analysis of isolated integrin-based adhesion complexes at the membrane. All secondaries were conjugated with horseradish peroxidase.

Primary Antibody	Species	Company/ Cat. No.	Dilution	Secondary Antibody	Species	Company/Cat. No.
ITG αv	Rabbit	Abcam/ ab179475	1:1000	anti-rabbit IgG	Goat	ProteinSimple/ DM-001
ITG α5	Rabbit	Abcam/ ab150361	1:1000	anti-rabbit IgG	Goat	ProteinSimple/ DM-001
ITG β3	Rabbit	Abcam/ ab179473	1:75	anti-rabbit IgG	Goat	ProteinSimple/ DM-001
ITG β1	Mouse	Thermo/ 14-0299-82	1:25	anti-mouse IgG	Goat	ProteinSimple/ DM-002

Table S5. Primary and secondary antibodies used for immunofluorescence staining displayed in Fig. 5.

Primary Antibody	Species	Company/ Cat. No.	Concentration used	Secondary Antibody	Species	Company/ Cat. No.	Concentration used
LM609 (active ITG αvβ3)	Mouse	Abcam/ ab190147	1:250	anti-mouse IgG Alexa 488	Goat	Invitrogen/ A32723	1:500
JBS5 (active ITG α5)	Mouse	Santa Cruz/ sc-59762	1:500	anti-mouse IgG Alexa 488	Goat	Invitrogen/ A32723	1:500
AIIB2 (active ITG β1)	Rat	DSHB University of Iowa	1:250	anti-rat IgG Alexa 488	Goat	Invitrogen/ A48262	1:500
Vinculin	Rabbit	Abcam/ ab129002	1:250	anti-rabbit IgG Atto 647	Goat	Rockland/ 611-156-122	1:2500
Vinculin	Mouse	Sigma/ V9131	1:1000	anti-mouse IgG Alexa 488	Goat	Invitrogen/ A32723	1:500
Paxillin	Rabbit	Abcam/ ab32084	1:250	anti-rabbit IgG Atto 647	Goat	Rockland/ 611-156-122	1:2500
Zyxin	Rabbit	Abcam/ ab229757	0.3ug/mL	anti-rabbit IgG Atto 647	Goat	Rockland/ 611-156-122	1:2500

Table S6. Primary and secondary antibodies used for immunofluorescence staining and confocal imaging for endosomal vesicle and integrin internalization studies in Fig. 6.

Primary Antibody	Species	Company/ Cat. No.	Concentration used	Secondary Antibody	Species	Company/ Cat No.	Concentration used
LM609 (active ITG αvβ3)	Mouse	Abcam/ ab190147	1:100	anti-mouse IgG Alexa 488	Goat	Invitrogen/ A32723	1:500
JBS5 (active ITG α5)	Mouse	Santa Cruz/ sc-59762	1:500	anti-mouse IgG Alexa 488	Goat	Invitrogen/ A32723	1:500
AIIB2 (active ITG β1)	Rat	DSHB University of Iowa	1:250	anti-rat IgG Alexa 488	Goat	Invitrogen/ A48262	1:500
EEA1	Rabbit	CST/ 3288S	1:200	anti-rabbit IgG Atto 647	Goat	Rockland/ 611-156-122	1:2500
Rab7	Rabbit	CST/ 9367S	1:200	anti-rabbit IgG Atto 647	Goat	Rockland/ 611-156-122	1:2500